NASA/TP–2002-211850

Design and Development of a Deep Acoustic Lining for the 40- by 80-Foot Wind Tunnel Test Section

Paul T. Soderman, Fredric H. Schmitz, Christopher S. Allen, Stephen M. Jaeger, Joe N. Sacco, Marianne Mosher, and Julie A. Hayes

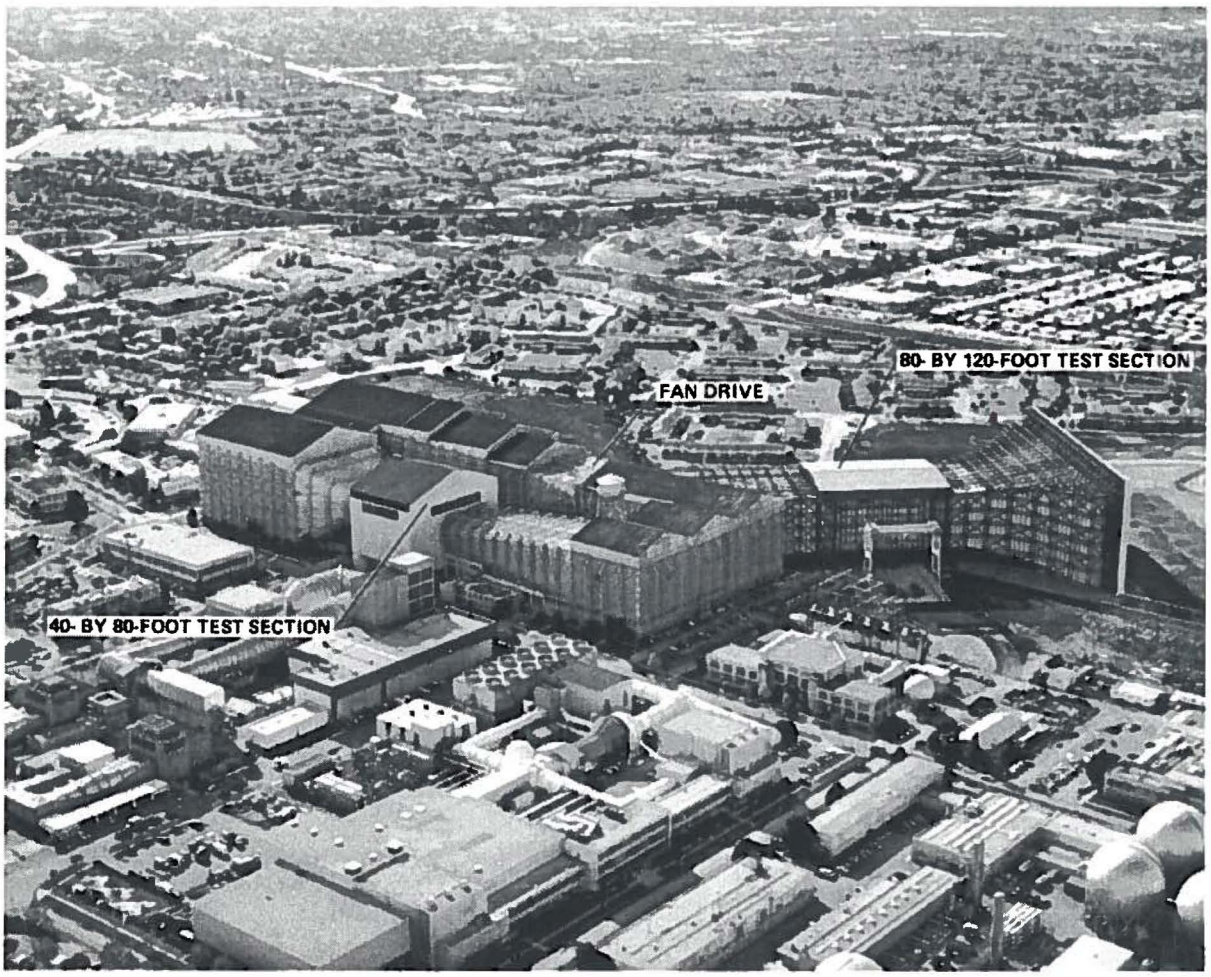

November 2002

The NASA STI Program Office . . . in Profile

Since its founding, NASA has been dedicated to the advancement of aeronautics and space science. The NASA Scientific and Technical Information (STI) Program Office plays a key part in helping NASA maintain this important role.

The NASA STI Program Office is operated by Langley Research Center, the Lead Center for NASA's scientific and technical information. The NASA STI Program Office provides access to the NASA STI Database, the largest collection of aeronautical and space science STI in the world. The Program Office is also NASA's institutional mechanism for disseminating the results of its research and development activities. These results are published by NASA in the NASA STI Report Series, which includes the following report types:

- TECHNICAL PUBLICATION. Reports of completed research or a major significant phase of research that present the results of NASA programs and include extensive data or theoretical analysis. Includes compilations of significant scientific and technical data and information deemed to be of continuing reference value. NASA's counterpart of peer-reviewed formal professional papers but has less stringent limitations on manuscript length and extent of graphic presentations.

- TECHNICAL MEMORANDUM. Scientific and technical findings that are preliminary or of specialized interest, e.g., quick release reports, working papers, and bibliographies that contain minimal annotation. Does not contain extensive analysis.

- CONTRACTOR REPORT. Scientific and technical findings by NASA-sponsored contractors and grantees.

- CONFERENCE PUBLICATION. Collected papers from scientific and technical conferences, symposia, seminars, or other meetings sponsored or cosponsored by NASA.

- SPECIAL PUBLICATION. Scientific, technical, or historical information from NASA programs, projects, and missions, often concerned with subjects having substantial public interest.

- TECHNICAL TRANSLATION. English-language translations of foreign scientific and technical material pertinent to NASA's mission.

Specialized services that complement the STI Program Office's diverse offerings include creating custom thesauri, building customized databases, organizing and publishing research results . . . even providing videos.

For more information about the NASA STI Program Office, see the following:

- Access the NASA STI Program Home Page at *http://www.sti.nasa.gov*

- E-mail your question via the Internet to help@sti.nasa.gov

- Fax your question to the NASA Access Help Desk at (301) 621-0134

- Telephone the NASA Access Help Desk at (301) 621-0390

- Write to:
  NASA Access Help Desk
  NASA Center for AeroSpace Information
  7121 Standard Drive
  Hanover, MD 21076-1320

NASA/TP–2002-211850

Design and Development of a Deep Acoustic Lining for the 40- by 80-Foot Wind Tunnel Test Section

Paul T. Soderman
Ames Research Center, Moffett Field, California

Fredric H. Schmitz
University of Maryland, College Park, Maryland

Christopher S. Allen
Ames Research Center, Moffett Field, California

Stephen M. Jaeger
AerospaceComputing, Inc., Ames Research Center, Moffett Field, California

Joe N. Sacco and Marianne Mosher
Ames Research Center, Moffett Field, California

Julie A. Hayes
Signalscape, Inc., Raleigh, North Carolina

National Aeronautics and
Space Administration

Ames Research Center
Moffett Field, California 94035-1000

November 2002

Acknowledgments

For a good part of the development program, Sandy R. Liu, who has since left government service, ably led the acoustic research reported here. The Ames Modification Project Office, staffed by numerous dedicated engineers, did an outstanding job managing this complex project. Dave Hickey and Dan Martin provided the boundary-layer data included here.

Available from:

NASA Center for AeroSpace Information
7121 Standard Drive
Hanover, MD 21076-1320
(301) 621-0390

National Technical Information Service
5285 Port Royal Road
Springfield, VA 22161
(703) 487-4650

Table of Contents

Summary

A deep, sound absorbent wall lining has been designed and installed in the National Full-Scale Aerodynamics Complex (NFAC) 40- by 80-Foot Wind Tunnel (40x80) test section at NASA Ames Research Center to create a nearly anechoic space for aeroacoustic research studies of aircraft models. To accommodate the lining, the test-section pressure shell was moved to the outside of the ring girders that surround and support the test section. Fiberglass wedges were installed in the cavity created between the flow boundary and pressure shell. The wedges are protected from the airflow by a porous interface at the flow boundary. The resulting acoustic lining is nominally 42 in. (1.07 m) deep except in certain shallow areas over structural beams, turntable apparatus, and diffuser inlet. The deep lining encircles the 83-ft long (25.3-m) test section and is joined to a 6-in. (15.2-cm) deep shallow lining that extends 20 ft (6.1 m) into the diffuser inlet for a total treated length of 103 ft (31.4 m) streamwise. The lining is faired to the original wind tunnel duct at the entry and exit of the test section.

The lining design method is described along with key results from extensive laboratory studies of the lining components. (Field data were obtained later and reported in refs. 1 and 2.) Much effort was put into optimizing the flow/lining interface that was required to protect the absorbent lining while satisfying structural, aerodynamic, and acoustic requirements. In particular, the floor panels were designed to carry loads from personnel and man-lifts without reflecting significant acoustic energy or causing excessive streamwise pressure drop. To handle these conflicting requirements, numerous porous materials and support structures were evaluated experimentally. The final design has a nominally 68%-open perforated steel sheet diffusion-bonded to a fine wire mesh screen and supported by an open grating. The unit is suspended over an egg-crate-type arrangement of 4- by 4-ft compartments (1.22- by 1.22-m) that contain eight fiberglass wedges each. Each 4- by 4-ft compartment is sealed on the sides and bottom to prevent air from circulating within the extended lining. The unusual depth of the lining will allow acoustic measurements to be made from very low to ultrasonic frequencies. The unique flow interface is designed to maintain good flow quality up to the 40x80 maximum speed of 300 knots.

Nomenclature

b	bar width or edge-to-edge hole spacing in perforated metal sheet, in. (cm)
c	sound speed, ft/sec (m/sec)
d	hole diameter of perforated metal sheet or distance, in. (cm)
f	frequency, Hz
h	lining depth, in. (cm)
H	acoustic pressure transfer function based on the ratio of ensemble averaged cross-spectra and auto-spectra data
L	center-to-center hole spacing of perforated metal sheet or lining length, in. (cm)
Lp	sound level relative to 20 μPa, dB
P	porosity of perforated metal sheet, i.e., ratio of open area to total area, percent
PLL	perpendicularly layered lining
R_f	flow resistance, cgs rayls
S	autopower spectrum of acoustic pulse incident on sample
U	mean velocity, ft/sec (m/sec)
y	perpendicular distance from lining surface, in. (cm)
α	lining sound absorption coefficient $= \frac{\textit{absorbed acoustic energy}}{\textit{incident acoustic energy}}$
ρ	air density, lb sec^2/ft^4 (kg/m^3)
Θ	acoustic incidence angle relative to surface normal, deg

Introduction

In recent years, the National Full-Scale Aerodynamics Complex (NFAC) 40- by 80-Foot Wind Tunnel (40 x 80) has operated with a 6-in. deep (15.2-cm) bulk-fiberglass acoustic lining in the test section to create a nearly anechoic space for aeroacoustic studies of aircraft models in simulated flight (see figs. 1 and 2). The floor lining included 1.5-in. deep (3.8-cm) support slats, so the fiberglass was only 4.5 in. (11.4 cm) deep on the floor. Because the test section is closed, the 3 lb/ft^3 (48 kg/m^3) fiberglass lining was protected from the airflow by a 40%-open-area perforated metal face sheet backed by a fiberglass cloth. Reference 3 describes the lining specifications and performance. The 6-in. (15.2-cm) lining served well for

small-scale model testing where frequencies of interest were generally above 1 kHz. (The physical cross section of the 40 x 80 was, in fact, 39 by 79 ft because of the acoustic liner.)

However, NASA management, spurred largely by F. Schmitz, former Director of Aeronautics at Ames Research Center, decided that future advances in aeroacoustic research would require a much-improved acoustic environment in the 40 x 80, especially with regard to large-scale powered models of all types. Rotorcraft and large jet testing in particular would benefit from improved sound absorption at low frequencies, though small-scale high-frequency aeroacoustic simulation is still a strong requirement.

To achieve high-quality acoustic performance over a wide frequency range, Ames initiated an ambitious design and development program to deepen and improve the acoustic lining without compromising the aerodynamic performance of the facility. The crux of the plan devised by Schmitz et al. (ref. 4) was based on the fact that the test-section pressure shell was constructed with four external 36-in. deep (91.4-cm) ring girders. With removal of the original pressure shell and installation of a new pressure shell on the outside surface of the ring girders, a deep space becomes available for an acoustic lining, and the original 40- by 80-ft (12- by 24-m) cross section is retained as the aerodynamic test section. However, the ring girders would reflect sound. By locating the flow surface 6 in. (15.2 cm) from the ring-girder inner surfaces, those reflections would be attenuated by the 6-in. (15.2-cm) treatment. A 42-in.-deep (1.07-m) lining could then be installed between the ring girders to leave a 39- by 79-ft (11.9- by 24.1-m) aerodynamic cross section. Several of NASA's advisory groups concluded that such a large-scale acoustic facility would be an essential asset to the nation's technological infrastructure. To that end, full-scale design was initiated in 1991, and demolition work on the test section was commenced in late 1995. The wind tunnel was reactivated in 1998.

Prior to the demolition, Ames personnel conducted an extensive series of studies and experiments for the purpose of designing the optimum acoustic lining. The optimization was constrained by available project funds, aerodynamic flow quality, and structural integrity of the facility.

The purpose of this report is to summarize the results of those studies and the resulting lining design while giving emphasis to the acoustic performance. Aerodynamic performance and structural specifications are described briefly. Others will report the aerodynamic design and testing; a thorough acoustic calibration of the treated test section was conducted and reported in references 1 and 2. A summary of the present report is presented in reference 5.

In parallel with the acoustic modifications described here, the NFAC fan-drive control system was improved for low-speed operation. Previous studies had shown that significant reductions in fan noise could be achieved at low to moderate test section airspeeds by operating the variable-speed/variable-pitch fans at low speed and high blade angle (ref. 3). Incorporating digital electronics into the motor control system expanded that part of the fan-operating envelope.

Wind Tunnel Environment

The Ames 40- by 80-Foot Wind Tunnel is a closed-circuit, closed-test-section facility (fig. 3). The 80- by 120-foot test section, also shown in figure 3, shares the same drive system, but is not part of the study described here. Top airspeed in the 40 x 80 is 300 knots or Mach 0.45. The wind tunnel is often used for aircraft landing and takeoff simulations and for studies of propulsion/airframe integration. Aerodynamic and acoustic studies are commonly made of unpowered or powered models using jet engines, propellers, rotors, fans, or high-pressure propulsion simulators. Fixed and moving in-flow microphones and phased microphone arrays are used to identify and record the model noise (ref. 4).

Six 40-ft-diameter (12.2-m), electrically powered fans constitute the drive section (fig. 4). As part of the acoustic modification project, low-speed fan-power capacity was increased. Since the fan blades are variable pitch and variable speed, minimizing blade rotational speed and maximizing blade angle (refs. 3, 6) can optimize thrust, noise, and power consumption. The drive-fan modification will decrease background noise in the test section at low to moderate airspeeds (refs. 3, 6, 7).

Eight large vortex generators at the diffuser entrance just downstream of the test section (fig. 5) energize flow along the diffuser walls. Because of their potential acoustic reflections, the vortex generators were moved 22 ft (6.7 m) downstream in order to reduce reflections into the test section. Wrapping them with acoustic material can be done in the future if necessary. We determined experimentally that other flow devices in the facility such as corner vanes are too far from the test section to be significant acoustic reflectors.

Design Goals

The primary project design goal was to create a sound absorbent test-section lining that would be operational

from 80 Hz to 20 kHz with a minimum of 90% energy absorption at those limits and as close to 100% absorption as practical between those limits. Furthermore, good absorption is desirable out to 80 kHz. Thus, the lining below the surface layer was designed to absorb 99% of the acoustic energy between 80 Hz and 20 kHz. The goals required much effort on the transmission of sound through the surface layer into the lower lining. In the turntable region, which has areas less than 42 in. (1.07 m) deep, the low-frequency limit for 90% absorption was set at 200 Hz. For certain shallow areas such as the diffuser inlet, the low-frequency limit was relaxed to 500 Hz.

For good flow quality over the speed range from 0 to 300 knots, a low-drag lining surface with small boundary-layer growth was required. Also, pressure gradients or cross-flows caused by large models must not create unusual flows through the lining or other flow anomalies in the test section. Therefore, the porous interface between the airstream and the deep acoustic lining required an engineering compromise. Accordingly, the interface material was designed to allow sound waves to pass through the interface with little energy reflected back to the test section interior, and at the same time, constrain the free airstream in the test section and support loads.

Structurally, the floor lining was designed to be robust and capable of supporting work crews and heavy equipment in the test section. This requirement led to a floor designed to carry (1) a point load of 1,800 lb (8,006 N) on an 8- by 8-in. (20.3- by 20.3-cm) area spaced no closer than 4 ft (1.22 m) on center, and (2) a uniform load of 200 lb/ft^2 (9,576 N/m^2).

Design Approach

Several unusual designs were evaluated early in the program, including removable modules, tensioned wire mesh over wedges, and working floors that folded into the walls to expose wedges. These were all rejected because of complexity, cost, or failure to satisfy one or more of the aerodynamic, structural, or acoustic requirements. It was extremely difficult to find a surface that was transparent to sound yet capable of carrying the structural loads without compromising the flow field. In the end, the design process proceeded toward a semi-permanent modular lining designed to satisfy the above requirements.

Schmitz et al. (ref. 4) described the conceptual design of the test section lining and history of the program, which is summarized here. To meet the sound absorption criterion down to 100 Hz for large rotor or jet work, absorbent wedges or bulk treatment in large depth are required. To protect the lining from airflow, a porous surface with low acoustic impedance is needed. Normally, sound absorption to 20 kHz is adequate but, for scale-model testing, 80-kHz performance was desired. However, this high-frequency requirement did not drive the lining design, because air absorption of reflected energy at high frequencies is strong in facilities as large as the 40 x 80, and surface absorption is less critical than it is in the audible range. At 50 kHz, for example, air absorption is 0.5 dB/ft (1.6 dB/m) on a standard day. Thus, reflected sound travels farther and gets absorbed faster by air than does direct sound. In addition, linings that absorb well at 20 kHz should also absorb well at higher frequencies. The limiting factor for good absorption occurs when the acoustic wavelength becomes comparable to the distance between the holes of perforated surface layers (ignoring thickness effects). Based on the final design, that wavelength is 0.03 in. (0.76 mm) or 448 kHz.

Testing Approach

To achieve the design goals, the project was organized as follows:

1. The project team conceived various lining designs.
2. Small-scale testing was initiated to evaluate the acoustic and aerodynamic performance of the designs.
3. Low-frequency sound absorption was measured with large impedance tubes.
4. High-frequency absorption was measured using a pulse-reflection technique.
5. Material flow resistance was checked for uniformity and for predicting absorption using empirical models.
6. Drag, boundary-layer growth, and pumping of airflow into the lining were measured in wind tunnels.
7. Structural integrity was evaluated by analysis and shake tests.
8. Lining designs, which performed well in the preceding tests, were integrated into large coupons, and installed in the 40 x 80 floor for evaluation before tunnel operations were stopped for the construction phase.
9. Finally, the optimum components were chosen for fabrication and installation in the 40- by 80-Foot Wind Tunnel.

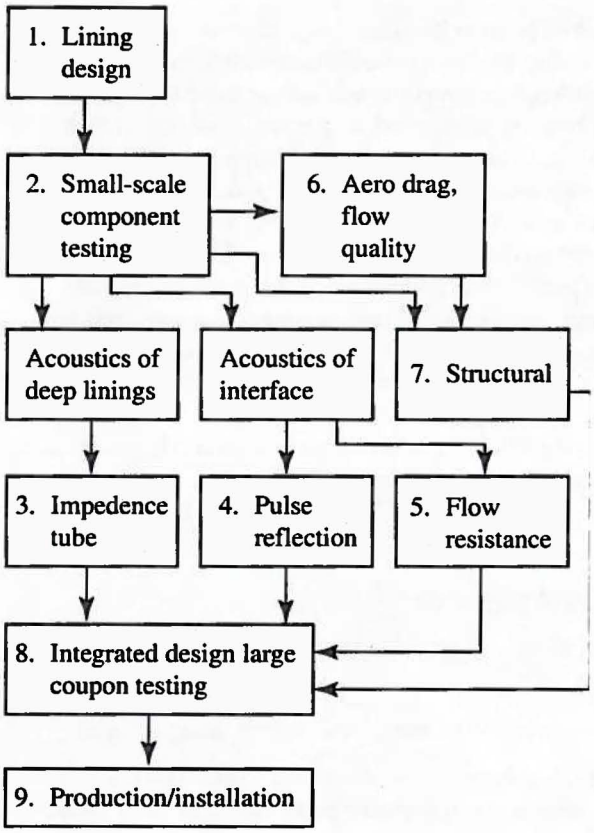

Lining Location

The location of the 40 x 80 acoustic lining is illustrated in figure 6. The deep lining is installed in the test section between the inlet contraction and start of the diffuser, a distance of 83 ft (25.3 m). The interior dimensions of the test section have been maintained save for a 6-in. (15.2-cm) lining intrusion into the original 40 x 80-ft cross section needed to cover certain beam surfaces and other hard points. Thus, the clear dimensions of the cross section are 39 by 79 ft (11.9 by 24.1 m).

The upstream edge of the lining is faired to the inlet contraction with a 12-ft-long (3.7-m) steel ramp, an improvement over the previous 1.5-ft-long (45.7-cm) ramp that generated sharp pressure gradients. The turntable area and structural beam surfaces have less than a 42-in.-deep (1.07-m) treatment, as will be illustrated in a later section. The 6-in.-deep (15.2-cm) surface treatment also extends 20 ft (6.1 m) into the diffuser so that microphones can be placed in that area to capture noise radiated from the test section. The downstream edge of the diffuser lining is faired to the diffuser with a 6-ft-long (1.8-m) ramp. Hence, a total length of 103 ft (31.4 m) is acoustically treated all around the test section perimeter; the inlet and exhaust ramp fairings remain untreated.

No other aerodynamic sections of the circuit (inlet contraction, diffuser, etc.) require modifications to maintain the flow quality in the test section.

Lining Modules

To avoid secondary flows within the lining that may occur because of pressure variations at the flow/lining interface, the deep lining is divided into 4-ft (1.2-m) square modular compartments that are sealed on the four sides and bottom (fig. 7). Over any one compartment, the static pressure induced by typical models will be fairly constant at the flow/lining interface. The 0.19-in.-thick (4.8-mm) steel sides of the modules (air dams) also carry loads to the 0.31-in.-thick (7.9-mm) steel pressure shell. The resulting egg-crate-type design was integrated into the 40 x 80 test section as an efficient structural design that was rigid and easy to standardize. A ballistically tolerant material was also integrated into selected parts of the test section for safety during rotorcraft and engine testing.

Candidate Designs for Deep Lining

We considered at least four deep-lining designs for filling the modular compartments. As shown in figure 8, the designs were (1) a single-layer bulk lining, (2) a multi-layered bulk lining, (3) a "poor man's wedge," more properly called by Ver a perpendicularly layered lining (PLL) (ref.8), and (4) a classic wedge system.

Reference will be made to (1) Owens Corning fiberglass products OCF 701/711, 1.5 lb/ft^3 (24 kg/m^3), 6,000 mks rayls/m* nominal flow resistivity; and (2) OCF 703/713, 3 lb/ft^3 (48 kg/m^3), 27,000 mks rayls/m nominal flow resistivity.

Single-layer bulk lining

A uniform layer of low-density bulk material is the least expensive method for sound absorption. For best acoustic absorption, the material must be quite light. A deep uniform lining therefore requires an internal structure to support it. Initial studies (ref. 8) of OCF 711 and OCF 703 fiberglass blankets 36-in. (0.914-m) deep were not promising, as shown in figure 9(a), which compares performance of bulk fiberglass with a wedge and the perpendicularly layered absorber to be discussed. Though inferior to the other absorbers, the lighter bulk fiberglass performance is similar to that shown by the prediction curve based on the model of Mechel and Ver, which used

* mks rayl has units of pressure/velocity = N•sec/m^3
cgs rayl = dyne•sec/cm^3

an empirical prediction for the fiberglass propagation constant and characteristic impedance (ref. 9). The prediction method is described in part A of the appendix.

However, Ver and Howe (ref. 10) found other bulk materials such as steel wool and Johns-Manville sliver, a lightweight long-fiber fiberglass filter product that performed better, as shown in figures 10(a) and (b); however, there were still bothersome dips in the absorption at low frequency. Note the effect of depth and density of steel wool in figure 10(a). Figure 10(c) shows the effect of needled stainless steel felt.

None of the bulk absorbers was quite as good as the simple wedge. Even packing lightweight Manville sliver around a wedge as shown in figure 10(d) slightly degraded performance except at frequencies below 100 Hz and, therefore, did not merit the extra expense.

Multi-layer bulk lining

Calculations of multi-layer lining absorption were made using the impedance model of Dunn and Davern (ref. 11). The model assumes that the layers are parallel to the back wall, as shown in figure 8. However, predicted performance was not as good for the multi-layer bulk lining as that expected from standard fiberglass wedges. Consequently, experimental testing of multi-layer absorbers oriented parallel to the back wall was not pursued.

Perpendicularly layered lining (PLL)

The design concept of the PLL is illustrated in figures 8 and 9. The PLL consists of vertically spaced layers of bulk acoustic material separated by layers of air or very-low-impedance material such as steel wool. The layers are perpendicular to the lining surface. The PLL design is related to that of multi-depth, multi-density fiberglass stacks used to line some anechoic chambers (ref. 12).

Figure 9(a) suggests that the performance of the PLL approaches that of the wedge design. However, further studies by Ver and Howe (ref. 10) illustrated in figures 11(a)-(c), show a low-frequency penalty for alternating layers of medium-fine steel wool and fiberglass that is alleviated somewhat by the use of coarse steel wool (fig. 11(c)), but not eliminated. And the promise of achieving large cost savings by using the PLL system is offset by the problem of finding a good practical material to act as the low-impedance layer between the acoustically absorptive layers and by the problem of adding the structure needed to support the vertical layers. Finally, there is concern that high-frequency sound might reflect from the blunt tips of the absorbent layers.

Wedges

Wedge systems are used in most anechoic chambers. They have the geometric advantage that, except for very low frequencies, waves reflecting from one wedge tend to hit the adjacent wedge and work into the valleys rather than reflecting back toward the source.

Ver (ref. 8) and Ver and Howe (ref. 10) evaluated many wedge designs in a low-frequency test program. Figure 12(a) summarizes results for an OCF 703 wedge (3 lb/ft^3 (48 kg/m^3)) with a 4-in. (10.2-cm) air gap behind the wedge. The nominal flow resistivity was 27,000 mks rayls/m. The sound absorption was very good down to 100 Hz. The wedge tip angle was 23°, though that variable was not evaluated. Figure 12(b) is a photo of this type wedge as configured for a coupon test in the 40 x 80 test section to be discussed.

Absorption of a similar wedge with an OCF 703 tip and a lower density base (OCF 701, 1.5 lb/ft^3 (24 kg/m^3), 6,000 mks rayls/m nominal) had an absorption coefficient 0.03 higher than a uniform OCF 703 wedge at 80 Hz, a small improvement not justified economically. Because of the excellent performance and reasonable cost, we chose the 3 lb/ft^3 (48 kg/m^3) fiberglass wedge for the deep lining.

Flow/Lining Interface: Aerodynamics

The first testing to develop the acoustically transparent wall system was done in the United Technologies Research Center's open-jet anechoic wind-tunnel facility (ref. 13). A mock-up of a typical interface panel over a deep cavity filled with a wedge-like structure was constructed and placed parallel to the flow on one side of the open jet.

Several panel surfaces were evaluated to determine the sensitivity of the boundary-layer characteristics to the cavity interface. This testing confirmed that the interface design was feasible, but also that it was critical to the aerodynamic performance of a deep lining. Results showed that flow over the porous interface tended to pump in and out of the cavity, which caused large boundary-layer growth. With a grating below the interface, the pumping was complicated by aeroacoustic resonance in the grating. Both effects could be controlled by low-flow resistance cloth positioned close to the flow-surface boundary. Sound absorption material in the cavity was also required. These preliminary results led to a series of more detailed aerodynamic studies which are described later.

Flow/Lining Interface: Low-Frequency Performance

No Grating

In addition to the evaluation of the sound-absorbent materials described above, Ver was contracted to test a great variety of flow/lining interface materials in a large impedance tube; some of the results were reported in references 5 and 7. For this discussion, the flow/lining interface is defined as the lining top surface layer(s) above the wedges not including support structure.

The low-frequency measurements were made with a fiberglass wedge mounted in a long 12-in.-square (30.5-cm) impedance duct. Various surface treatments representing the lining/flow interface were placed across the duct at the wedge tip.

Figures 13(a) and (b) show that a very porous flow/lining interface can be almost transparent to low-frequency sound. For example, the installation of a porous sintered-metal sheet (Technetics FM 125, 10 cgs rayls flow resistance*) at the wedge tip caused only a small reduction in absorption (fig. 13(a)). Bauer (ref. 14) found a similar result in his study of acoustically transparent wind-tunnel walls, which were made from a composite of perforated steel and sintered metal mesh with a flow resistance of 10 cgs rayls. Ver (ref. 8) found that good absorption was also achieved with a 40%-open perforated plate with 2 cgs rayls cloth below (fig. 13(b)). Figure 13(c) shows that a nominal 68%-open perforated metal sheet with a fiberglass cloth on top (2 cgs rayls) had absorption performance close to that of the baseline wedge. However, all these interface surfaces need a structural support grating, which complicates the acoustical design and performance.

With grating

For structural support, a grating of vertical steel slats spanning each 4-ft-module (1.2-m) is needed under the porous face sheets. Three different types of grating were designed for the various locations of the test section surfaces (fig. 14). The floor grating slats run cross-stream and the wall grating slats run streamwise. The floor grating is the heaviest in order to provide support of personnel and equipment such as man-lifts. A low wall area is designed to support personnel only, and the upper wall/ceiling needs to carry only aerodynamic loads.

Figure 15(a) illustrates the floor grating, which must support the heaviest load and, therefore, has a 12-gauge slat with spacing of 1.38 in. (3.5 cm). The low-wall medium grating has 2-in.-deep (5.1-cm) 12-gauge slats on 3-in.-centers (7.6-cm) (fig. 15(b)). The ceiling/upper wall lightweight grating has fewer and shorter 16-gauge grating slats as shown in figure 15(c). Many of the acoustical studies were focused on the difficult problem of minimizing sound reflection by the floor panels.

Figure 16(a) shows that a 68%-open 12-gauge steel perforated sheet supported by the floor grating allowed good low-frequency, normal-incident sound absorption. However, aerodynamic studies showed that a porous membrane is required at the surface to prevent airflow from pumping in and out of the lining, which would aggravate the boundary-layer growth and increase the drag. Fiberglass cloth under the grating (2 cgs rayls) only degraded the mid-frequency sound absorption to 98%, (fig. 16(b)), a slightly stronger effect than shown in figure 13(b) for cloth and plate without grating. However, cloth is difficult to install, as will be discussed later.

As an alternative to cloth, it was found that a fine-mesh, stainless-steel screen above or below the perforated plate worked well aerodynamically, but reduced the mid-frequency sound absorption coefficient to 0.94 (fig. 16(c)). The flow resistance of the screen/perforated plate combination was estimated to be 25 cgs rayls. Wire-mesh optimization is discussed in detail later in the section on high-frequency performance.

It was speculated that part of the absorption penalty shown in figure 16(c) came from acoustic energy trapped by the screen and grating slats. Therefore, an attempt was made to regain some of the performance by installing light fibrous material between the floor grating slats. Figure 17(a) shows that fine steel wool (flow resistivity estimated at 750 mks rayls/m) stuffed in the grating without screen or perforated cover brought the mid-frequency sound-absorption coefficient to 0.96. However, a grating filler material with too much flow resistance, such as OCF 701 fiberglass, had quite a detrimental effect, as shown in figure 17(b). A lighter material in the grating, Scotch Brite, a fiber abrasive, had a lesser effect on sound absorption (fig. 17(c)).

The final product evaluated was Fibair, a lightweight fiberglass filter material, placed in the grating as shown in figure 17(d). That material, in combination with a screen and perforated plate, had an absorption of about 95% in the mid-frequencies. A layer of Fibair compressed from 2.75 in. (7.0 cm) to 2 in. (5.1 cm) has a flow resistance of about 1.3 cgs rayls at an airspeed of 1 m/s. (Doubling the compression raises the flow resistance to 2.7 cgs rayls.) The acoustic performance was further improved by

---

* The convention of cgs rayls for flow resistance (10 cgs rayls equals 100 mks rayls) is used.

perforating the grating slats to alleviate resonance between the slats and is described below.

Thus, Fibair as a grating filler was slightly more effective acoustically than steel wool. Furthermore, it was decided that with vibration over time, steel wool fibers might slough particles that could be detrimental to the wind-tunnel drive motors or other electrical systems in the wind tunnel. The electrical windings of the drive motors, for example, might attract such particles. Fiberglass particles would be much more benign.

Flow/Lining Interface: High-Frequency Performance

Pulse-reflection method

To study high-frequency reflections from the numerous flow/lining interface designs considered during the project, Wilby et al. (ref. 15) and Wilby and Wilby (refs. 16-22) were contracted to evaluate a large number of interface samples using an acoustic pulse-reflection technique. The technique they developed was more reliable for high-frequency studies than the standard impedance-tube method and allowed incidence angle variation.

The interface specimens were mounted over a 48- by 48- by 42-in.-deep box (1.07- by 1.22- by 1.07-m) filled with a fiberglass wedge assembly that acted as an anechoic termination. That is, reflections were predominantly from the simulated flow/lining surface, which typically was a perforated or sintered plate in contact with a low-resistance screen or cloth.

The two-microphone system Wilby et al. (ref. 15) devised is illustrated in figure 18. A high-frequency speaker generated a short chirp pulse about 10.5 ft (3.2 m) from the specimen. The pulse was measured by two microphones mounted at grazing incidence to the speaker: a reference microphone fixed above and to the side of the test-specimen center and a movable microphone mounted to the specimen box. The reference microphone was out of the path of the direct sound, but could always be related to the incident sound at position 1 using a calibrated transfer function developed during the setup:

$$H_{ref,1}(f) = \frac{< S_1(f)\, S_{ref}^{*}(f) >}{< S_{ref}(f)\, S_{ref}^{*}(f) >} \qquad (1)$$

Equation (1) uses cross-spectral notation and represents an average over an ensemble of repeated tests. At a later time, data from the reference microphone could be related to the incident wave by

$$S_1(f) = S_{ref}(f) H_{ref,1}(f) \qquad (2)$$

As the specimen box was rotated, the movable microphone was positioned in line with the reflected waves on a constant-radius arc centered at the acoustic impact point. Hence, the microphones captured the direct and reflected sound at various incidence angles without the necessity of correcting for microphone directivity. A transfer function between the reflected wave at position 2 and the reference microphone was found experimentally:

$$H_{ref,2}(f,\theta) = \frac{< S_2(f,\theta) S_{ref}^{*}(f) >}{< S_{ref}(f) S_{ref}^{*}(f) >} \qquad (3)$$

and

$$S_2(f,\theta) = S_{ref}(f) H_{ref,2}(f,\theta) \qquad (4)$$

Finally, the acoustical absorption coefficient is given by

$$\alpha(f,\theta) = 1 - \left[\frac{d_1 + d_2}{d_1 - d_2}\right]^2 \frac{\left\langle |S_2(f,\theta)|^2 \right\rangle}{\left\langle |S_1(f)|^2 \right\rangle} \qquad (5)$$

where the last term represents a ratio of 10 ensemble averages of autospectra of the reflected and incident waves. The parameters d_1 and d_2 are the distances from the source to the lining and from the lining to the microphone, respectively (see fig. 18). The acoustic impedance was also calculated.

The source signal was a chirp pulse generated by a rapid frequency sweep from 0 to 50 kHz which, because of tweeter response roll-off, yielded an effective pulse about 1.6 msec long and contained energy between 3 and 30 kHz. Figure 19 illustrates a typical pulse and reflection from a sample. The direct and reflected pulses were isolated using a time window and then Fourier transformed for input into equation (1). The time window was tapered by a 0.04-msec-long cosine squared function at the beginning and end of the window. The resulting absorption data were plotted in both narrowband and third-octave bandwidths. The third-octave absorption coefficients, which were computed from third-octave sound spectra, smoothed out some of the frequency-dependent variations since the data were averaged over each band. The general trends are thereby more obvious.

High-frequency data repeatability

Pulse-reflection data repeatability was first checked by repeating runs without moving the apparatus. Figure 20(a) shows that the absorption data repeated nicely. Next, we moved the panels in increments of a few inches without changing the measurement setup. Because of variations in

panel geometry such as flatness, screen flow resistance, and support-slat position, the reflections did change somewhat, as shown in figure 20(b). The pulse-reflection results cannot be expected to be more accurate than the scatter in figure 20(b). As a final check on the experimental method, absorption data were compared with theoretical predictions for simple fiberglass linings, as discussed in part B of the appendix.

Previous 40 x 80 lining surface

Figure 21 shows absorption coefficients for the bare, uncovered anechoic termination and for the anechoic termination covered by a sample covering similar to the previous 40 x 80 floor flow/lining interface. The interface was a 40%-open perforated plate over a grating of 1.5-in.-deep (3.8-cm), 0.125-in.-thick (3.2-mm) slats spaced on 1.25-in. centers (3.2-cm). The sample was exposed to acoustic pulses at several incident angles. The data show that at frequencies between 4 kHz and 20 kHz this moderately porous interface degraded the sound absorption. Hence, a search for a more acoustically transparent interface that maintained good test section flow quality was initiated. To simplify the discussion, only the data at a single incidence angle will be shown in most cases.

Metal face sheets without grating

Figure 22 shows that porous Feltmetal (Technetics FM125) with a flow resistance of 10 cgs rayls allowed lining sound-absorption values of about 95%, which was better than that of two other materials—Purolator Poroplate, a 32%-open perforated plate bonded to a stainless-steel fine screen (also 10 cgs rayls) and Almute sintered porous aluminum over a 0.5-in. (1.27-cm) honeycomb layer (30 cgs rayls). However, there were concerns about the integrity of these materials without a supporting structure, so other solutions were sought, including a grating under the face sheet.

Metal face sheets with grating

Figure 23 shows that a support grating caused degradation of the FM125 Feltmetal performance shown in figure 22. However, a 16-gauge 68%-open perforated plate attained much better sound absorption despite the addition (on top) of a fine screen (200 x 200 wires per inch, flow resistance unknown). Gratings will be examined in more detail, but first some face-sheet effects will be discussed.

Effect of face-plate porosity

The above results agree with the intuitive idea that better acoustic performance of an absorbent lining can be achieved by increasing surface porosity. This effect was explored systematically on a 16-gauge (0.063-in.-thick (1.59-mm)) perforated metal plate without grating (ref. 13). Hole diameter was held at 0.188 in. (4.76 mm). Figure 24 shows that sound absorption increased with porosity, and that porosity must be at least 50% to achieve 90% sound absorption up to 17 kHz. Since 90% is only marginally acceptable, the 68%-porous sheet was chosen for the final design because of its superior performance. This performance is offset somewhat by the need for greater support of highly porous sheets.

The openness of a nominal 68%-porous plate is illustrated in the photograph and schematic of figures 25 and 26. Because of deformations caused by the punching process, the porosity can vary from 65% to 68%.

Effect of face-plate hole diameter

The effect of hole diameter was measured for the 0.25-in. and 0.063-in. thick (6.35-mm and 1.59-mm) steel plates without grating as shown in figure 27. Porosity was held between 48% and 51%. The data suggest that smaller holes transmit sound better than larger holes, particularly at high frequency. Related to this parameter (diameter) is the thickness of material between the holes—the greater the thickness (large holes), the greater the reflections. However, that parameter is not represented directly in the equations of Guignouard (ref. 23) and others described in the appendix.

Effect of face-plate hole orientation on boundary layer

The final lining design had holes overlapped in the flow direction as illustrated in figure 26. That orientation was chosen because of fluid mechanic studies, which showed that hole orientation was an important factor in flow drag. The alternate orientation is holes lined up as if the flow were left to right in figure 26. Measurements of boundary-layer growth along a 9.8-ft (3-m) long section of perforated plate and screen installed flush with a wind-tunnel wall and positioned over a 22-in.-deep (56-cm) cavity resulted in the following boundary-layer momentum thickness growth.

		Boundary-layer Momentum Thickness Growth
Holes overlap	Screen on flow side	0.206 in. 5.23 mm
Holes line up	Screen on flow side	0.233 in. 5.92 mm
Holes overlap	Screen below plate	0.290 in. 7.37 mm
Holes line up	Screen below plate	0.304 in. 7.72 mm

Since drag is linearly related to momentum thickness, the upper table indicates a 13% drag increase owing to holes aligned relative to holes overlapped if the screen is on the flow side. The lower table shows a 5% drag increase for the same conditions, except for the screen positioned below the perforated plate. Examination of the hole pattern in figure 26 suggests that the streamwise distance between holes is the parameter controlling momentum thickness. With holes aligned, the streamwise distance between holes was only 0.03 in. (0.75 mm). With holes overlapped, the streamwise distance between holes was 0.187 in. (4.74 mm). Thus, the flow interaction between holes and the effective roughness are less with holes overlapped. The effect of screen placement on drag is discussed further in the section on screen-position effects.

The above data were obtained with a 12-gauge, 66%-open perforated plate (0.188-in., 4.8-mm holes on 0.22-in., 5.6-mm staggered centers) and the 200 x 600 mesh Dutch twill screen described below. The screen was glued to the 39-in.-wide by 9.8-ft-long plate (99 cm by 3 m), which was supported by a grating. Airspeed was 200 knots. Because drag and power are linearly related, the above data also indicate that, for a constant velocity, the power absorbed by a test section lined with the above material would have the same dependence on hole orientation as did the drag.

Effect of face-plate thickness

Figure 28(a) shows that for a 48%-open perforated plate (ref. 16) without grating, the thicker the plate the greater the reflection and lower the sound absorption of the lining. The effect was strongest at normal incidence. The same trend with thickness was found with 68%-open sheet, though the effect was weaker (fig. 28(b)).

Effect of incidence angle

The transmission of sound into an absorbent lining increases significantly as incidence angle is changed from normal or 0° to 30°, as shown in figure 29 for various plates without grating. These data show a clearer trend with incidence than figure 21, which also showed incidence effects but had the complication of grating effects. The absorption should increase until incidence angles exceed 80° and then drop precipitously as reported by Cops and Myncke (ref. 24) and suggested by the results of Soderman (ref. 25). Pierce (ref. 26) showed theoretically that the increased absorption with incidence angle is a result of the impedance boundary condition necessary to balance the viscosity and thermal conduction of energy incident and absorbed at the wall. He shows that plane wave absorption reaches a maximum at a high incidence angle and then drops to zero at grazing incidence.

Effect of support grating slat height

Grating slat height was varied from 0.5 in. (1.27 cm) to 2.0 in. (5.08 cm), but the resulting absorption coefficients do not show a consistent trend (fig. 30). The shortest slats seem to have had the least reflection, as might be expected. These data were acquired without a porous cover plate over the grating.

Effect of slat spacing

Figure 31 shows that grating-slat spacing of 4.74 in. (12.1 cm) allowed good transmission of sound energy into the lining. Below that spacing, reflections are seen at certain frequencies, particularly for 1.188-in. (3.0-cm) slat spacing. The dips in the curve at 6.3 kHz correspond to a frequency at which the wavelength or half-wavelength are comparable to the slat spacing, which is indicative of an acoustic resonance condition. Resonance is a natural phenomenon and difficult to avoid.

Effect of slat orientation

Sound rays at oblique incidence can enter the grating parallel to the slats or, in the extreme, perpendicular to the slats. Figure 32 shows that sound entering in a plane perpendicular to the slats is reflected much easier than sound rays entering in a plane parallel to the slats, as might be expected. The apparent blockage seen by a sound ray is greater in a plane perpendicular to the slats. All other data in this section were taken for the worst case which is sound rays in a plane perpendicular to the slats.

Effect of slat porosity

As mentioned above, the high-frequency data suggested that the slat reflections were not solely from the top slat edges, but were related to a resonance between slats. This is also evident in figure 33, which shows that simply perforating

the slats (40%- and 46%-open area) reduced the reflections significantly. This is a very beneficial effect and it was incorporated in the final grating design.

Effect of bulk material between slats

As found in the low-frequency studies previously discussed, the high-frequency data also indicate that grating slats tend to trap and reflect acoustic energy, an effect that can be alleviated by perforating the slats and by installing light fiberglass fill between the slats (ref. 14). This must be done with care: too dense a fill will cause reflections. Figures 34(a) and (b) show that both light fiberglass (OCF 701) and stainless-steel wool (fine grade 0) stuffed between the slats improved the high-frequency sound absorption of the lining contrary to the low-frequency penalty of OCF 701 shown in figure 17(b). Presumably, the acoustic energy can enter the material at high frequency, but the impedance of OCF 701 (6,000 mks rayls/m nominal) is too great for low-frequency sound to enter easily.

As reference, the narrowband absorption data and normalized impedance data for these configurations are presented in figures 34(c)-(e). Note the smoothness of the absorption and impedance data with steel wool between the grating slats.

After evaluating several other products, a light fiberglass material called Fibair was incorporated in the final grating design. Figures 35(a) and (b) show Fibair being installed in the floor and wall grating prior to installation of the porous covering. These photos also illustrate the porous slats described above, as well as other components such as the metal rods used to support the slats and the cylinders in each corner through which the panel is bolted to the wind tunnel. A light wire mesh is mounted behind the Fibair to retain the fibrous material.

Effect of cloth and porous plate

Aerodynamic studies showed that a porous membrane adjacent to the porous metal face sheet was necessary to prevent airflow from pumping in and out of the lining and thus control the resultant boundary-layer growth. The first choice for this membrane was fiberglass cloth because of its potentially favorable acoustic effects.

However, fiberglass cloth had several practical drawbacks. On the floor, it would have had to be protected by placing it between the porous face sheet and grating. And, unless it was bonded to the face sheet, it would sag between the grating slats and could lose its aerodynamic effectiveness. Gluing the cloth to the porous face sheet proved to be very difficult without clogging the face sheet holes, which would affect the sound transmission. Figure 36 shows that a non-bonded fiberglass cloth (J.P. Steven 1675, 2 cgs rayls flow resistance) draped between the perforated sheet and grating actually improved the high-frequency sound absorption of the lining. But adhesives for holding the cloth to the porous faceplate degraded the high-frequency sound absorption despite attempts to apply it spread lightly or in fine lines.

Furthermore, the cloth would interfere with welding of the face sheet and grating. For these reasons, metal screens were evaluated to overcome these in situ performance limitations of fiberglass cloth.

Wire screen glued to perforated plate

Figure 37 shows high-frequency sound absorption of fiberglass wedges with a fine-mesh stainless-steel screen (Dutch twill: 200 warp by 600 shute wires/in., 0.0024-in. and 0.0018-in. diameter, 8-10 cgs rayls at 100 cm/sec airspeed) epoxy bonded to the underside of a 68%-open 12-gauge perforated plate. Figure 38 illustrates the geometry of the screen and perforated plate. Different amounts of adhesive were used in the experiment, which resulted in flow resistance for the plate/screen combination that varied from 13.9 to 17.9 cgs rayls. Although the flow resistance variations were not great, the heavily glued screen had a detrimental effect on sound absorption above 7 kHz, because the adhesive had bled into the porous plate, effectively reducing the diameter of each orifice (fig. 37).

Wire screen diffusion bonded to perforated plate

The final solution to the problem of attaching the wire screen to the perforated plate was to diffusion-bond the two materials. Diffusion bonding is a process whereby two metals in contact in an inert atmosphere are subjected to high temperature just below their melting points, which causes them to weld together. In principle, a very clean, strong bond between screen and plate can be achieved.

However, there are production difficulties. To produce a large batch of plates and screens, fibrous sheets are placed between each pair of screen/plate combinations to keep them isolated. The fibrous sheets are a source of contamination. Much care is required to prevent fibers from adhering to the screen during diffusion bonding, which causes increased flow resistance and sound reflection. A cleaning process was incorporated in the production process, but it was imperfect, and flow resistance of the plate/screen varied somewhat as discussed in the next section.

Wire screen/porous plate flow resistance

The acoustic performances of various diffusion-bonded plate/screen combinations is shown in figure 39 for two different plate thicknesses. The screen mesh variations resulted in flow-resistance values varying from 5.0 to 29.2 cgs rayls. Note that a panel without a screen had absorption similar to the diffusion-bonded plate/screen with low flow resistance. Clearly, the high-flow-resistance screen had the greatest degradation of sound absorption. Flow resistance does not seem to have a strong effect until values exceed 15 cgs rayls, but there may be geometric parameters involved with these data. Consequently, we decided to test a number of screen/plate flow resistivities using a common mesh geometry and various amounts of contaminant in the screen to cause variations in flow resistance.

Figure 40 shows the effect of diffusion bonding on the high-frequency sound absorption of several plate/screen combinations where the plate/screen flow resistance varied from 16.9 to 25.7 cgs rayls because of variability in particle contamination of the screens; that is, the mesh geometry was common to all curves. In figure 40(a) the high-flow-resistance screens had the poorest performance at high frequency. This is more clearly illustrated in figure 40(b), which is a cross-plot of absorption coefficient versus flow resistance. Because the absorption starts to decrease at about 21 cgs rayls, production panels with flow resistance above that value would be expected to have below average performance.

Effect of wire screen position

The pulse-reflection tests showed that the position of the screen relative to the perforated plate affected the acoustic performance. Screen below the plate (lining side) achieved somewhat better absorption compared to placement of the screen above the plate (sound side). Figures 41 and 42 illustrate this for 12-gauge and 16-gauge perforated plates, respectively. The effect of position is slightly stronger for the thicker plate. The acoustic mechanism for the change in absorption with screen position is unknown. We measured no difference in flow resistance for the two screen orientations.

The screen position also had a strong effect on fluid mechanics. The wind-tunnel study described above of boundary-layer growth along a 9.8-ft-long (3-m) section of perforated plate and screen installed flush with the wind-tunnel wall and positioned over a 22-in.-deep (56-cm) cavity resulted in the following boundary-layer momentum thickness growth.

Screen on flow side of perforated plate	Growth of momentum thickness = 0.206 in. (5.23 mm)
Screen under perforated plate	Growth of momentum thickness = 0.290 in. (7.37 mm)

Since drag is linearly related to momentum thickness, the data indicate a 41% drag reduction owing to screen placement on the flow side of the perforated plate relative to screen placement below the plate. Clearly, the perforated plate was much rougher than the fine-mesh screen.

The above data were obtained with a 12-gauge, 66%-open perforated plate (0.188-in. holes (4.8-mm) on 0.22-in. staggered centers (5.6-mm)) and the 200 x 600 mesh Dutch twill screen described above. The screen was glued to the 39-in.-wide by 9.8-ft-long plate (99-cm by 3-m), which was supported by a grating. The plate holes overlapped in the flow direction, as shown in figure 26. Airspeed was 200 knots. Because drag and power are linearly related, the above data also indicate that for a constant velocity, the power absorbed by a test section lined with the above material would be 41% lower with the screen on the flow side relative to screen under the perforated plate.

Production panels and cleaning effectiveness

Because some of the production panels were partially contaminated with glass fibers, an attempt was made to improve panel performance by cleaning the screens. Figure 43(a) shows a production panel with high, but unknown flow resistance that resulted in comparatively low sound absorption as shown. However, the cleaning process, which involved wiping with acetone and drying with compressed air, actually reduced the sound absorption. Presumably, the glass fibers were deeply imbedded in the fine screen weave.

There is also a concern that wind tunnel operation might contaminate the panels. For example, jet engines are often operated in the 40 x 80. To simulate this degradation, a panel was contaminated by soot from burning jet fuel (JP5), acoustically tested, and then cleaned with acetone, blown with shop air, and tested again. The soot build up was thick and left the panel black, a situation much worse than anticipated from normal wind tunnel operation. Figure 43(b) shows that this contamination had a severe effect on sound absorption, but that it could be adequately removed. Consequently, regular testing and cleaning of the installed acoustic lining in the wind tunnel may be required. However, no progress has been made in restoring good acoustic performance of panels contaminated during the fabrication process.

40- by 80-Foot Wind Tunnel "coupon" tests

As a check on the validity of the small-sample testing prior to fabrication of the immense acoustic lining (20,566 ft^2, 1,911 m^2), two aerodynamic and acoustic full-scale "coupon" tests were conducted in the 40-by 80-Foot Wind Tunnel test section before the tunnel was shut down for the modification. A portion of the test section floor 8 ft wide by 20 ft long (2.44 m by 6.10 m) was cut to accept a series of 10 acoustic modules, each 4 ft square (1.22 m) as shown in figures 44(a) and (b). The wind-tunnel pressure shell was lowered in that area such that each module was a 42-in.-deep cavity (1.07-m) bounded by the 0.188-in.-thick (4.8-mm) air dam and 0.313-in. (7.9-mm) steel bottom pressure plate similar to the illustration in figure 7(b). Two of the modules contained a test section ring girder whose surface was 6 in. (15.2 cm) below the floor surface and represented an area of minimal lining depth to be investigated.

Only static acoustic tests were possible with the modified high-frequency pulse-reflection test rig illustrated in figure 45 (see ref. 16). Because the test sample could not be rotated relative to the sound source, as in the laboratory setup, four loudspeakers were mounted on an arc so that acoustic incidence could be varied. The arc was in a plane perpendicular to the grating slats. Direct and reflected acoustic pulses were measured using two microphones. Aerodynamic studies were made of boundary-layer growth and other fluid-mechanic parameters to be reported by others.

Comparisons of coupon data with the laboratory test-rig results are shown in figure 46 for the floor and wall linings as defined at that time. However, exact duplication of previously tested configurations was not possible. The closest lab data were taken without slats below the cover plate. The somewhat poorer absorption measured during the coupon tests was partially a result of the slat configuration and fiberglass filler which, in this application, was detrimental to absorption contrary to the laboratory results shown in figure 34(a). It is possible that the filler was packed too tightly.

Generally speaking, the coupon study was more beneficial to the aerodynamic studies of the lining than to the acoustics. The acoustic performance was generally good, considering the differences between the laboratory and coupon configurations. However, it became clear that it is difficult to match idealized laboratory performance in the full-scale facility.

Shallow beam coverings

During the coupon test, sound-absorbent measurements were made over the 24-in.-wide (0.61-m) ring-girder surface, which was 6 in. (15.2 cm) below the floor. In that area, the beams were covered with 3-in. (7.6-cm) bulk fiberglass and 3-in.-deep grating and porous plate. The data showed that the OCF 701 fiberglass was superior to OCF 703 at that depth, but the converse was true at greater depths. Cloth wrapping slightly degraded the sound absorption. The following criteria were chosen for covering structural elements below the lining surface.

Depth	Fiberglass
$h < 6$ in.	OCF 701 (1 lb/ft^3) bulk
$6 \le h < 14$ in.	OCF 703 (3 lb/ft^3) bulk
$h \ge 14$ in.	OCF 703 wedge

Figure 47 shows that at the highest frequencies ($f = 16$ kHz and 20 kHz) absorption coefficients over the ring girder were 0.05 to 0.08 less than the absorption coefficients of the deep module. It is anticipated that the low-frequency sound below 1 kHz will tend to diffract around the beams. However, more detailed measurements will be made in this area during the wind-tunnel acoustic calibration following the lining installation.

Figure 48 illustrates the locations of shallow lining modules in the turntable area, which contains structural elements needed to support and rotate aircraft models.

Predicted Acoustic Performance

Pulse-reflection data and a number of analytical prediction methods—for low- and high-frequency sound absorption of a perforated plate spaced above an anechoic termination—are compared in the appendix. The complexities of the screen, grating, and grating filler could not be modeled. But for a simple perforated plate, the impedance model of Guignouard et al. (ref. 23) resulted in normal incident absorption coefficients which were closer to the data than the results of other models evaluated, as shown in figure 49 and discussed in the appendix.

Flow-Induced Noise

It is well known that turbulent boundary layers can generate significant noise. Noise generation can be further increased if flow over highly porous cavities or silencers causes flow-induced resonance. Soderman (ref. 27) showed that flow over acoustic baffles could generate loud tones unless steps were taken to dampen the cavity oscillations or to uncouple the flow excitation from the cavity resonance, which should be easily accomplished by the

fiberglass wedges. Hence, flow noise in the test section should not be amplified by the lining, and should be less than expected for flow over a rough surface.

Diffuser Lining

A 6-in.-deep (15.2-cm) fiberglass lining has been installed in the diffuser inlet for a distance of 20 ft (6.1 m) as an extension to the deep lining. Figure 50(a) shows the lining plan view. The total length of test section acoustic treatment is 100 ft (30.5 m), not including the metal ramps which fair the lining into the wind-tunnel surface at the upstream and downstream edges. Figure 50(b) shows an elevation view of the diffuser lining.

Vortex generators and diffuser columns

Figure 50(a) also illustrates two of the eight vortex generators located at the diffuser inlet. The devices have been relocated to a station 4.5 ft (1.37 m) downstream of the diffuser lining ramp as shown. The devices were wrapped with 3-in.-thick (7.6-cm) polyurethane foam to minimize acoustic reflections back into the test section. The foam was covered with 0.25 by 0.25 in. (6 by 6 mm) fine steel mesh for protection. The vortex generators are 3.83 ft (1.17 m) high and have an 11.42 ft (3.48 m) chord and 25 in. (63.5 cm) maximum thickness. However, it was later discovered that the foam could not be retained in the presence of wind, so the vortex generator wrap was removed and the devices moved another 22 ft (6.7 m) downstream (ref. 1).

A series of support columns on the diffuser centerline commence 45 ft (13.7 m) downstream of the diffuser ramp (fig. 50(a)). These columns were not modified and should have negligible effect on test-section acoustics.

Final Design

Through experimental testing and analysis, a deep acoustic lining for the 40 x 80 test section was designed to provide suitable sound absorption between 80 Hz and 20 kHz or higher. The design is a complex trade-off between acoustic and aerodynamic performance, structural integrity, ease of manufacture, and cost. The acoustic performance was the focus of this report.

Throughout most of the test section, the acoustic lining is composed of 4-ft-square (1.22-m) modular compartments 42 in. (1.07 m) deep that contain 36-in.-tall (91.4-cm) wedges over a 4-in. (10.2-cm) air gap; they are protected from the airstream by a porous interface. The module geometry and specifications are illustrated in figure 51(a). The eight wedges within each module are alternately oriented streamwise and cross-streamwise so as to block acoustic waves traveling parallel to a wedge valley. Each 4- by 4-ft module (1.22- by 1.22-m) is surrounded by 0.188-in.-thick (4.8-mm) steel panels, or air dams, which carry loads and prevent airflow between modules. The air dams and other exposed surfaces are shielded by cloth-wrapped fiberglass to minimize acoustic reflections (OCF 701 fiberglass and J.P. Stevens 1675 fiberglass cloth). The fiberglass wedges are also protected by fiberglass cloth and, over the cloth, a light wire mesh with 0.5-in. (1.3-cm) wire spacing.

In the floor and turntable area the total lining depth varies from the full 42 in. (1.07 m) to 5.5 in. (14.0 cm), and over the ring girders the lining depth is 5.5 in. (14.0 cm). Therefore, the turntable and ring-girder areas will have below average sound absorption relative to the rest of the test section.

Because of differing structural requirements, there are three interface panel designs, as illustrated in figures 51 (b) - (d). The floor surface is a 68%-open, perforated 12-gauge (0.105-in.-thick, (2.66-mm)) steel sheet with a fine-mesh stainless-steel screen diffusion-bonded to the underside for flow control. The sheet is supported by a steel grating with 2-in. (5.1 cm), 12-gauge, 51%-open porous slats spaced 1.38 in. (3.5 cm) apart.

The lower wall panels (fig. 51(c)) utilize the same interface sheet supported by similar porous steel grating slats spaced 3 in. (7.6 cm) apart. The ceiling panels (fig. 51(d)), which actually extend down the sides of the test section (see fig. 14), are made from lighter 16-gauge (0.06-in.-thick (1.52-mm)) 68%-open perforated steel sheet with the same fine-mesh screen attached to the flow side. These panels are supported by 16-gauge 51%-open porous slats that are 1.25 in. deep (3.2 cm) on 6-in. centers (15.2 cm). The screen on the flow side of the perforated plate has less drag, but slightly poorer sound absorption than the screen under the perforated plate. A light fiberglass material (Fibair) is stuffed between the slats on all panels to minimize internal reflections.

The stainless-steel screen described above has a nominal flow resistivity of 8 to 10 cgs rayls. A 10-cgs-rayls screen bonded to a 68%-open perforated plate would have a flow resistance of about 10/0.68 = 14.7 cgs rayls. However, because of contamination during the diffusion-bonding process, the flow resistance of the screen/plate test samples varied from 16 to 26 cgs rayls, or sometimes even more. As a result, production panels with high flow resistance will have lower than average sound absorption locally. The test-section local and global acoustic performance will be documented during integrated system tests planned for the reactivation of the facility.

Concluding Remarks

The work described in this report has made effective use of design teams to build a state-of-the-art anechoic wind-tunnel facility. We evaluated many potential design solutions using engineering analysis and computational tools. Design alternatives were then evaluated using specially developed testing techniques. Large-scale coupon testing was then performed to develop confidence that the preferred design would meet the acoustic, aerodynamic, and structural objectives of the project. Finally, designs were frozen and the final product was installed in the wind tunnel.

The result of this technically ambitious project has been the creation of a unique acoustic wind tunnel. Its large test section (39 ft x 79 ft x 80 ft), potentially near-anechoic environment, and medium subsonic speed capability (M = 0.45) will support a full range of aeroacoustic testing—from rotorcraft and other vertical takeoff and landing aircraft to the takeoff/landing configurations of both subsonic and supersonic transports.

APPENDIX

PREDICTION METHODS FOR SOUND ABSORPTION OF ACOUSTIC LININGS

Current methods for predicting the sound absorption qualities of porous materials cannot model the complete wind-tunnel lining comprising the porous face sheet, screen, perforated wall grating, and fiberglass wedges. However, some components can be modeled, and the predicted performance gave credibility to the experimental methods described in this report.

Part A. Bulk Fiberglass Absorption: Low Frequency

Mechel and Ver (ref.9) employed regression constants from experimental data to compute the impedance and sound absorption of fibrous materials; we used them to predict the low-frequency sound absorption of certain 40x80 acoustic linings. The normal incidence absorption coefficient for a large flat absorber without covering and placed against a hard surface is given by

$$\alpha_n = \frac{4 Z_1 Z_0}{\left(Z_1' + Z_0\right)^2 + Z_1''^2} \tag{6}$$

where

α_n is the acoustic energy absorption coefficient (ratio of absorbed and incident energy)
Z_1 is the normal specific lining impedance
Z_1' and Z_1'' are the real and imaginary components of Z_1
$Z_0 = \rho_0 c_0$ is the characteristic impedance of air

and

$$Z_1 = Z_0\left[\left(1 + b'E^{-\beta'}\right) - jb''E^{-\beta''}\right]\coth(\Gamma_a d) \tag{7}$$

The complex propagation constant is

$$\Gamma_a = k_0 a'E^{-\alpha'} + j\left(1 + a''E^{-\beta''}\right) \tag{8}$$

where d is the lining depth

$E = \rho_0 f / R_1$ is a normalized frequency parameter

f is the frequency, Hz

R_1 is the lining flow resistivity, mks rayls/m

$k_0 = \omega / c_0 = 2\pi f / c_0$ is the acoustic wave number in air

and

$a', a'', \alpha', \alpha'', b', b'', \beta', \beta''$ are regression constants from table 8.2 in reference 9, which are reproduced below for mineral/basalt wool and fiberglass.

Regression Constants

Material	E region	a′	α′	a″	α″	b′	β′	b″	β″
Mineral/basalt Wool	E ≤ 0.025	0.322	0.502	0.136	0.641	0.081	0.699	0.191	0.556
	E > 0.025	0.179	0.663	0.103	0.716	0.0563	0.725	0.127	0.655
Glass fiber	E ≤ 0.025	0.396	0.458	0.135	0.646	0.0668	0.707	0.196	0.549
	E > 0.025	0.179	0.674	0.102	0.705	0.0235	0.887	0.0875	0.770

The above equations were coded to give the prediction curve in figure 9(a), which agrees well with impedance tube data for a 36-in.-deep OCF 701 bulk fiberglass lining with a density of 24 kg/m^3 and a flow resistivity of 6,000 mks rayls/m. Unfortunately, the prediction for OCF 703 (48 kg/ m^3, 27,000 mks rayls/m) differed considerably from the measured sound absorption. The computer code follows.

```
/*  MV_absorp.c                                                                    2/7/97
 *                                                                          Paul T. Soderman
 *                                                                  NASA Ames Research Center
 *  Think C compiler (ANSI C) for Macintosh
 */
/*****************************************************************************************
 *
 *  Program computes normal incidence sound absorption of bulk material based on the
 *  empiricial curve of Mechel and Ver (Noise and Vibration Control Engineering.
 *  Beranek and Ver, ed. Ch 8 Mechel and Ver.
 *  This code is commented to be ISO 9000 compliant. The author does not guarantee accuracy
 *  of the results nor that the code will run under all conditions.
 *
*****************************************************************************************/

#include <math.h>
#include <stdio.h>
#include <string.h>
#include <time.h>
#include <console.h>                    /* needed for output redirection using Think C and Mac    */

#define NFREQ           36                      /* number of frequencies                          */
float   alpha[NFREQ] = {0};                     /* array of sound absorption coeffs               */

char    file_name[30];                          /* string array of file name                      */
typedef struct
                {
                double  depth;                  /* lining depth, m                                */
                double  resist;                 /* lining resistivity, mks rayls/m    */
                } lining_t;

                                /* function prototypes                                    */
void    alpha_calc( lining_t, float*, long int* );
void    data_out( lining_t, float*, long int* );
int     make_file( lining_t, char*, float*, long int* );
```

```
int       print_file( char* );
void      skip_line( void );
lining_t lining;

int main()
{

        char      menu( char ),
                  i = '1',                                  /* menu number                          */
                  **dummy;                                  /* dummy argument for access to I/O     */
        char      *ptr_file_name;                           /* pointer to file name string          */
        long int *ptr_freq;                                 /* pointer to freq array                */
        float     *ptr_alpha;                               /* pointer to alpha array               */
        int       count = 0,                                /* record counter                       */
                  printout = 1;                             /* printer control constant             */
        long int freq[] = {25,31,40,50,63,80,100,125,160,200,250,315,400,500,630,800,
                           1000,1250,1600,2000,2500,3150,4000,5000,6300,8000,10000,12500,
                           16000,20000,25000,31500,40000,50000,63000,80000};
                                                            /* third oct center freqs               */

        ptr_freq = freq;                                    /* initialize pointers                  */
        ptr_alpha = alpha;
        ptr_file_name = file_name;

        while ( printout )
        {
                i = menu( i );
                switch ( i )
                {
                        case '1':
                                /* Call absorption calc routine and absorption array            */

                                printf( "\nCalculate sound absorption\n" );

                                printf( "\t%s", "Input lining depth, m " );

                                scanf( "%lf", &lining.depth );

                                printf(" \n\t%s", "Input material flow resistivity, mks rayls/m " );

                                scanf( "%lf", &lining.resist );

                                alpha_calc( lining, alpha, freq );

                                make_file( lining, ptr_file_name, alpha, freq );

                                skip_line();

                                break;

                        case '2':
                                data_out( lining, alpha, freq );

                                break;
```

```
                        case '3':
                                printf("\t %s \n", " choose file as standard input ");

                                printf("\t %s \n", " and console+printer for standard output ");

                                printf("\t %s \n \n", "hit return to start and finish this operation ");

                                scanf("%c", &i);

                                ccommand ( &dummy );
                                /* dialog box and I/O redirection options      */
                                /* must be last after declarations             */

                                printout = print_file( ptr_file_name );

                                break;

                        case '4':
                                exit (1);

                                break;
                }
        }
        return 0;
}

/*****************************************************************************************************
 Function menu() creates menus for user input and output manipulation.
*****************************************************************************************************/

char menu ( char ch )
{
        printf( "\n\n%s\n","NASA Ames Research Center" );

        printf( "%s\n","Record Database" );

        printf( "%s\n \n","Enter One Selection 1 - 4" );

        printf( "\t%s\n","1 - Input data, calculate results, make file" );

        printf( "\t%s\n","2 - Display results on screen" );

        printf( "\t%s\n","3 - Print output file and exit" );

        printf( "\t%s\n","4 - Exit program" );

        ch = getchar();

        skip_line();

        return ch;
}
```

```
/*****************************************************************************************************
* Function alpha_calc computes sound absorption of a bulk liner against a hard surface.
* Normal incidence sound is assumed. The alpha array is filled.
*
*****************************************************************************************************/

void alpha_calc( lining_t lining, float *ptr_alpha, long int *ptr_freq )
{
        const float rho = 1.225,        /* air density, kg/cu m                 */
                    co = 340.0,         /* sound speed, m/s                     */
                    pi = 3.141593,      /* pi                                   */
                    zo = 416.5,         /* char impedance of air, mks rayls     */
                    ap1 = 0.396,        /* regression constants for fiberglass  */
                    ap2 = 0.179,        /* table 8.2                            */
                    alfap1 = 0.458,
                    alfap2 = 0.674,
                    app1 = 0.135,
                    app2 = 0.102,
                    alfapp1 = 0.646,
                    alfapp2 = 0.705,
                    bp1 = 0.0668,
                    bp2 = 0.0235,
                    betap1 = 0.707,
                    betap2 = 0.887,
                    bpp1 = 0.196,
                    bpp2 = 0.0875,
                    betapp1 = 0.549,
                    betapp2 = 0.77;
        const double e = 2.1718282;
        double  ko,                     /* wave number in air                   */
                efreq,                  /* MV frequency constant                */
                gama_real,              /* propagation constant, real comp      */
                gama_imag,              /* propagation constant, imag comp      */
                zan_real,               /* matl char impedance, real comp       */
                zan_imag,               /* matl char impedance, imag comp       */
                z1n_real,               /* lining impedance, real comp          */
                z1n_imag;               /* lining impedance, imag comp          */
        int     i,                      /* loop counter                         */
                first = 1,              /* complex number flags                 */
                second = 2;
        long int ifreq;                 /* frequency parameter                  */
        double complex_hyper_cot( double X, double Y, int flag );

  for (i = 0; i < NFREQ; i++, ptr_alpha++, ptr_freq++)
  {
    ifreq = *ptr_freq;

    ko = 2.0 * pi * ifreq / co;

    efreq = rho * ifreq / lining.resist;

    if ( efreq <= 0.025 )
    {
       gama_real = ko * ap1 / pow( efreq, alfap1 ) * lining.depth;
```

```
            gama_imag = ( 1.0 + app1 / pow( efreq, alfapp1 )) * lining.depth;

            zan_real = 1.0 + bp1 / pow( efreq, betap1 );

            zan_imag = - bpp1 / pow( efreq, betapp1 );
        }
        else
        {
            gama_real = ko * ap2 / pow( efreq, alfap2 ) * lining.depth;

            gama_imag = ( 1.0 + app2 / pow( efreq, alfapp2 )) * lining.depth;

            zan_real = 1.0 + bp2 / pow( efreq, betap2 );

            zan_imag = - bpp2 / pow( efreq, betapp2 );
        }
        z1n_real = zan_real * complex_hyper_cot( zan_real, zan_imag, first );

        z1n_real -= zan_imag * complex_hyper_cot( zan_real, zan_imag, second );

        z1n_imag = zan_real * complex_hyper_cot( zan_real, zan_imag, second );

        z1n_imag += zan_imag * complex_hyper_cot( zan_real, zan_imag, first );

        *ptr_alpha = 4.0 * z1n_real;

        *ptr_alpha /= (( z1n_real + 1.0 ) * ( z1n_real + 1.0 ) + z1n_imag * z1n_imag );
    }
    return;
}

/*****************************************************************************************************
 * Function complex_hyper_cot computes the real and imaginary values of the hyperbolic
 * cotangent of a complex number.  The real or imaginary components are returned depending
 * on the flag sent to the function: 1 for real, 2 for imaginary.
 *
 *****************************************************************************************************

double complex_hyper_cot( double X, double Y, int flag )

{
        double  a,b,c,d,                /* parameters abcd for coth ratio        */
        value,                          /* return value (real or imaginary)      */
        e1;                             /* parameter for exp(x)                  */

        e1 = exp( X );

        a = e1 * cos( Y ) + cos( Y ) / e1;

        b = e1 * sin( Y ) - sin( Y ) / e1;

        c = e1 * cos( Y ) - cos( Y ) / e1;
```

```
        d = e1 * sin( Y ) + sin( Y ) / e1;

        if( flag == 1 )
                value = ( a * c + b * d ) / ( c * c + d * d);

        else
                value = ( b * c - a * d ) / ( c * c + d * d );

        return value;
}

/*****************************************************************************************************
 * Function make_file creates a file of frequencies and computed absortion coefficients.

 *****************************************************************************************************

int make_file( lining_t lining, char *ptr_file_name, float *ptr_alpha, long int *ptr_freq )

{
        int     i;
        time_t now;
        struct tm *date;
        char s[80];

        FILE    *fp;

        strcpy( file_name,"MV_sound_absorption" );

        now = time( NULL );

        date = localtime( &now );

        strftime( s, 80, "%x", date );

        strcat( file_name, s );

        printf( "\n\t%s\n" ,"make file" );

        if ( (fp = fopen(file_name, "w")) == 0 )
        {
                printf( "cannot open file %s to write\n",file_name );

                return 0;
        }

        fprintf( fp, " \n\n %s ", file_name);

        fprintf( fp, " \t%s ", " P. Soderman ");

        strftime( s, 80, "%a, %b %d, %Y %H:%M", date );

        fprintf( fp, "%s\n", s );

        fprintf( fp, " \t %s %3.1f %s \n ", "fiberglass depth = ", lining.depth, "m");
```

```
        fprintf( fp, " \t %s %3.1f %s \n \n ", "resistivity = ", lining.resist, "mks rayls/m" );

        fprintf( fp, " \t %s \n ", " Absorption coefficient (normal incidence) " );

        for ( i = 0; i < NFREQ; i++, ptr_freq++, ptr_alpha++ )
                fprintf( fp, " %5ld  %6.4f%c ", *ptr_freq, *ptr_alpha, (i%5==4 || i==NFREQ-1 ? '\n' : ' ' ));

        fclose( fp );

        return 1;
}

/*****************************************************************************************************
* Function print_file prints file created by make_file to standard output
*****************************************************************************************************

int print_file( char *ptr_file_name )
{

        FILE    *fp;
        int c;

        if ( (fp = fopen(file_name, "r")) == 0 )
        {
                printf( "cannot open file %s to read\n",file_name );

                return 0;
        }

        while( (c = fgetc(fp) ) !=EOF )
                putchar( c );

        fclose( fp );

        return 1;
}

/*****************************************************************************************************
* Function data_out prints computed output to screen
*****************************************************************************************************

void data_out( lining_t lining, float *ptr_alpha,  long int *ptr_freq )
{
        int     i;

        printf(" \n \n \t %s ", " Sound Absorption - normal incidence ");

        printf(" \t \t %s \n ", " P. Soderman ");

        printf( " \t %s %3.1f %s \n ", "fiberglass depth = ", lining.depth, "m");

        printf( " \t %s %3.1f %s \n \n ", "resistivity = ", lining.resist, "mks rayls/m" );
```

```
        printf( " \t %s \n ", " Absorption coefficient (normal incidence) " );

        for ( i = 0; i < NFREQ; i++, ptr_freq++, ptr_alpha++ )
                printf(" %5ld  %6.4f%c ", *ptr_freq, *ptr_alpha, (i%5==4 || i==NFREQ-1 ? '\n' : ' '));

        return;
}

/*****************************************************************************************
* Function skip_line reads and ignores all characters up to and including the first new-line
* character.  Use to clear input buffer.
*****************************************************************************************

void skip_line( void )
{
        while( getchar() != '\n' )
        ;
}
```

Part B. Analytical Model of Plate and Lining: High Frequency

Wilby and Wilby (ref. 18) evaluated a number of analytical models for the absorption of sound by porous materials spaced behind a perforated facing. The predictions were then compared with data from the high-frequency pulse test series. None of the models account for a grating between the facing and lining.
It is assumed that the acoustic impedance of a perforated plate can be taken in series with that of a backing lining.

$$\varsigma = \varsigma_l + \varsigma_p = \vartheta + i\chi \tag{9}$$

where

ς is the total specific acoustic impedance normalized by $\rho_0 c_0$

ς_l and ς_p are the normalized specific impedance of the back lining and perforated facing, respectively, and ϑ and ς are the real and imaginary components of ς.

Wilby and Wilby found that the real part of the normalized specific impedance of the back lining was essentially 1 and that the imaginary part was essentially zero (ref. 18). Furthermore, the impedance of a perforated plate located some distance from the back lining is dominated by the reactance. Thus, equation (9) simplifies to:

$$\varsigma = 1 + i\chi_p \tag{10}$$

and the absorption coefficient is given by

$$\alpha = 1 - \left| \frac{i\chi_p}{2 + i\chi_p} \right|^2 = \left(1 + 0.25\chi_p{}^2\right)^{-1} \tag{11}$$

Thus, it is necessary to obtain a relationship for χ_p.

Guignouard et al. (ref. 23) give the following expression for reactance of a perforated plate:

$$\chi_p = (k_0 / P)(t + 2\delta) \tag{12}$$

where

P = open area ratio
t = plate thickness
d = perforation hole diameter

and the end correction for a hole is

$$\delta = 0.24d\left(\pi^{0.5} - 2.5P^{0.5}\right) \tag{13}$$

which is taken from Ingard (ref. 28), but becomes negative for P > 0.503.

In another work from Ingard (ref. 29), the end correction is given as

$$\delta = \left(\pi d^2 P / 4\right)^{0.5} F(p) \tag{14}$$

where F(P) is described graphically and decreases as P increases so that F(P) = 0 when P = 1. This and other representations of end correction are illustrated in figure 52.

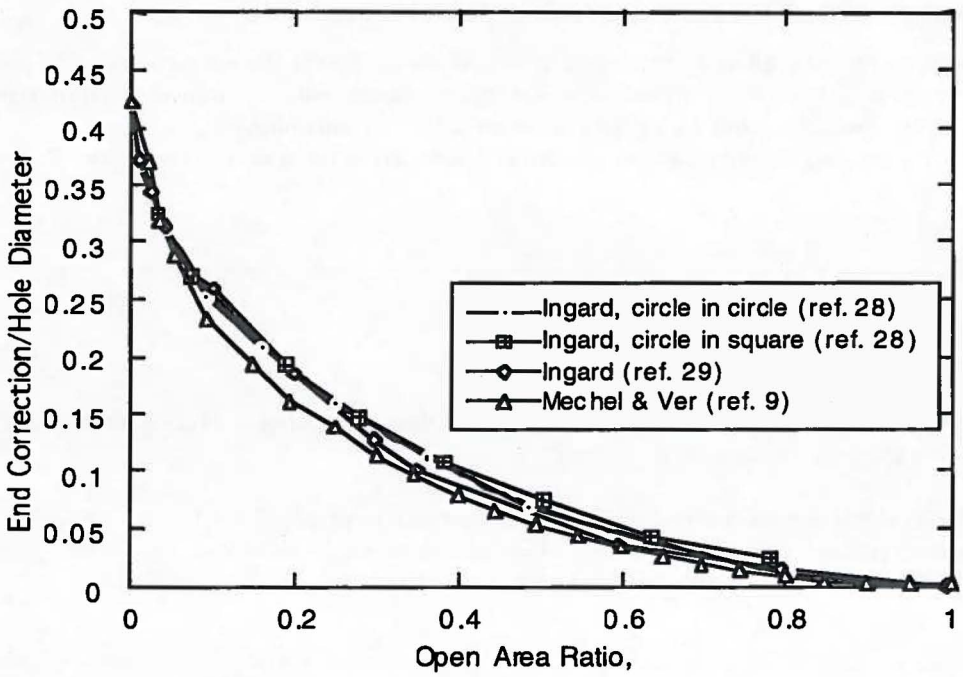

Figure 52. Comparison of end corrections for holes in a perforated plate (from ref. 17).

In addition to the above expressions for bulk absorbers, Mechel and Ver (ref. 9) have published two models for impedance of a perforated plate. One, according to Wilby and Wilby (ref. 18) is equivalent to equation 12. The second gives the impedance of perforated plate resonator covers exposed to various sound pressure levels and grazing flow speeds. For low sound pressure levels and zero flow:

$$\chi_p = (k_0 / P)\left[(8\nu/\omega)^{0.5}(1 + t/d) + t + 2\delta\right] \tag{15}$$

where

ν is the kinematic viscosity of air

and the appropriate end correction is

$$\delta = 0.425 d \phi(P) \tag{16}$$

where

$$\phi(P) = 1 - 1.47P^{0.5} + 0.47P^{1.5} \tag{17}$$

Figure 49 shows a comparison of measured sound absorption by Wilby and Wilby (ref. 15) with the above predictions of Guignouard et al. (ref. 23), Ingard (ref. 28), and Mechel and Ver (ref. 9). The Guignouard model agrees best with the data, particularly for the 16 gauge, 68%-open perforated plate.

References

1. Soderman, P. T.; Jaeger, S. M.; Hayes, J. A.; and Allen, C. S.: Acoustic Performance of the 40- by 80-Foot Wind Tunnel Test Section Deep Acoustic Lining. AIAA Paper 2000-1939. 6th AIAA/CEAS Aeroacoustics Conference, Lahaina, Hawaii, June 2000.

2. Soderman, P. T.; Jaeger, S. M.; Hayes, J. A.; and Allen, C. S.: Acoustic Quality of the 40- by 80-Foot Wind Tunnel Test Section After Installation of a Deep Acoustic Lining. NASA/TP—2002-211851.

3. Soderman, P. T.: Sources and Levels of Background Noise in the NASA Ames 40- by 80-Foot Wind Tunnel: A Status Report. NASA TM-100077, May 1988.

4. Schmitz, F. H.; Allmen, J. R.; and Soderman, P. T.: Modification of the Ames 40- by 80-Foot Wind Tunnel for Component Acoustic Testing for the Second Generation Supersonic Transport. 7th European Aerospace Conference, Toulouse-Labege, France, Oct. 1994.

5. Soderman, P. T.; Schmitz, F. H.; Allen, C. S.; Jaeger, S. M.; Sacco, J. N.; and Hayes, J. A.: Design of a Deep Acoustic Lining for the 40- by 80-Foot Wind Tunnel Test Section. AIAA Paper 99-1938, 5th AIAA/CEAS Aeroacoustics Conference, Seattle, Wash., May 10-12, 1999.

6. Soderman, P. T.; and Mort, K. W.: Aeroacoustic Characteristics of a Large, Variable-Pitch Fan System. Proceedings for Inter-Noise 83, vol. 1, Edinburgh, Scotland, July, 1983, pp. 123 - 125.

7. Hayes, J. A.; Allen, C. S.; Soderman, P. T.; and Jaeger, S. M.: Test Techniques and Instrumentation for Acoustic Studies in Wind Tunnels. ISA 41st International Instrumentation Symposium, Denver, Colo., May 1995.

8. Ver, I. L.: Initial Acoustical Design Study for Improving the Free-Field Acoustic Simulation Performance of the Test Section of the NASA Ames Full-Scale Wind Tunnel. Contract No. FF 8024, BBN Systems and Technologies Corp, July 1988.

9. Mechel, F.; and Ver, I.: Sound-absorbing Materials and Sound Absorbers. Ch. 9 in Noise and Vibration Control Engineering, L. Beranek and I. Ver, eds., John Wiley & Sons, Inc., 1992.

10. Ver, I. L.; and Howe, M. S.: Acoustic Lining Study for the 40- by 80-Foot Wind Tunnel. BBN Systems Report No. 7739 (NASA Contract NAS2-13461), Sept. 1992.

11. Dunn, I. P.; and Davern, W. A.: Calculation of Acoustic Impedance of Multi-layer Absorbers. Applied Acoustics, vol. 19, 1986, pp. 321-334.

12. Berhault, J. P.; Sunyach, M.; Arbey, H.; and Comte-Bellot, G.: Réalisation d'une chambre anéchoïque revetue de panneaux et destinée à l'étude des bruits d'origine aérodynamique (Design and Construction of an Anechoic Chamber Lined with Panels for Investigation of Aerodynamic Noise). Acustica, vol. 29, no. 2, 1973, pp. 69-78 (in French).

13. McCormick, D. C.: Aerodynamic Performance of Candidate Acoustic Linings for the NFAC 40x80-Ft Wind Tunnel. UTRC R93-970413-1, Aug. 1993, contract NAS2-13605.

14. Bauer, A. B.: Acoustically Transparent Walls for Aeroacoustic Wind Tunnel Applications. AIAA Paper 76-92, AIAA 14th Aerospace Sciences Meeting, Washington D.C., Jan. 1976.

15. Wilby, J. F.; White, P. H.; and Wilby, E. G.: Pulse Reflection Study of Acoustic Lining Coverings. AARC Report 137 (NAS2-13459), Atlantic Applied Research, May 1992.

16. Wilby, J. F.; and Wilby, E. G.: Lining Reflections at High Frequencies: Progress Report for Phase I. WA Report No. 103, (NAS2-13605), April 1993.

17. Wilby, J. F.; and Wilby, E. G.: Lining Reflections at High Frequencies - Phase II. WA Report No. 104, (NAS2-13605), Aug. 1993.

18. Wilby, J. F.; and Wilby, E. G.: Lining Reflections at High Frequencies - Phase IIA. WA Report No. 105, (NAS2-13605), Sept. 1993.

19. Wilby, J. F.; and Wilby, E. G.: Lining Reflections at High Frequencies - Phase III. WA Report No. 106, (NAS2-13605), Nov. 1993.

20. Wilby, J. F.; and Wilby, E. G.: Lining Reflections at High Frequencies - Phase IIB. WA Report No. 107, (NAS2-13605), Jan. 1994.

21. Wilby, J. F.; and Wilby, E. G.: Lining Reflections at High Frequencies - Phase IV. WA Report No. 108, (NAS2-13605), July 1994.

22. Wilby, J. F.; and Wilby, E. G.: Reflections of High-Frequency Sound from Perforated Plates with Diffusion-Bonded Screens. WA Report No. 126, (NAS2-13605), Sept. 1993.

23. Guignouard, P.; Meisser, M.; Allard, J. F.; Rebillard, P.; and Depollier, C.: Prediction and Measurement of the Acoustic Impedance and Absorption Coefficients at Oblique Incidence of Porous Layers with Perforated Facings. Noise Control Engineering Journal, vol. 36, no. 3, May-June, 1991, pp. 129-135.

24. Cops, A; and Myncke, H.: Determination of Sound Absorption Coefficients Using a Tone-Burst Technique. Acustica, vol. 29, 1973, pp. 287-296.

25. Soderman, P. T.: Oblique Incidence Sound Absorption of Porous Materials Covered by Perforated Metal and Exposed to Tangential Airflow. Inter-Noise 82, Proceedings vol. II, San Francisco, Calif., May 1982, pp. 401-404.

26. Pierce, A. D.: Acoustics – An Introduction to Its Physical Principles and Application. Ch. 10, Effects of Viscosity and Other Dissipative Processes, McGraw-Hill Book Co., N.Y., 1981.

27. Soderman, P. T.: Design and Performance of Resonant-Cavity Parallel Baffles for Duct Silencing. Noise Control Engineering, vol. 17, no. 1, July-August 1981, pp. 12-21.

28. Ingard, U.: On the Theory and Design of Acoustic Resonators. J. Acoust. Soc. of Amer., vol. 25, no. 6, Nov. 1953, pp. 1037-1061.

29. Ingard, U.: Perforated Facing and Sound Absorption. J. Acoust. Soc. of Amer., vol. 26, no. 2, Mar. 1954, pp. 151-154.

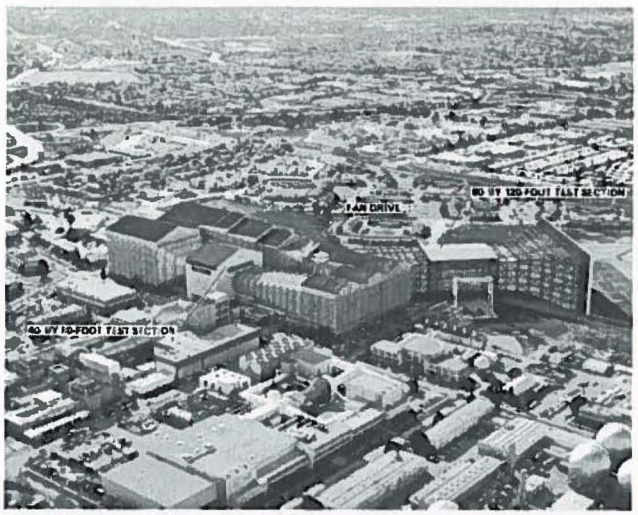

Figure 1. National Full-Scale Aerodynamics Complex (NFAC).

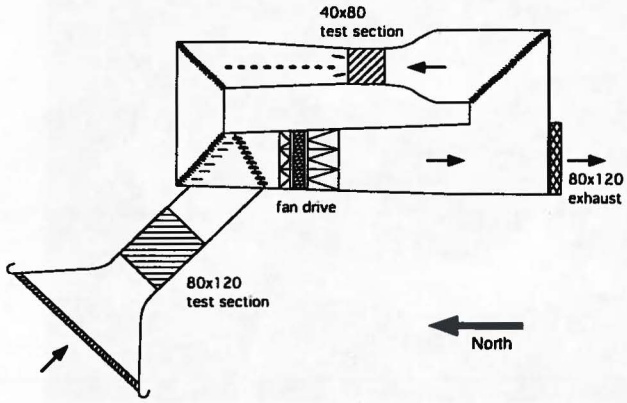

Figure 3. NFAC plan view.

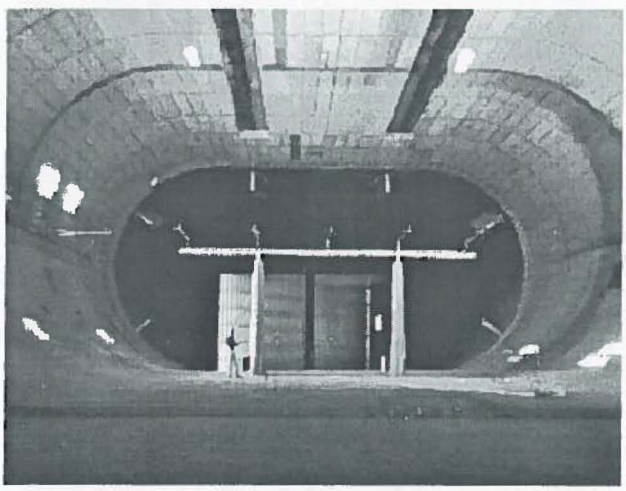

Figure 2. 40x80 test section showing the 6-in. (152-mm) deep absorbent wall lining prior to demolition and installation of the deep lining; view looking downstream.

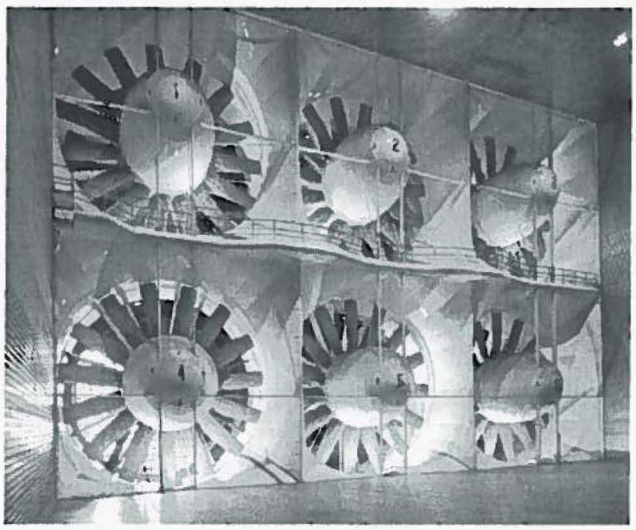

Figure 4. The six variable speed, variable blade-pitch drive fans; each fan is 40 ft (12.2 m) in diameter.

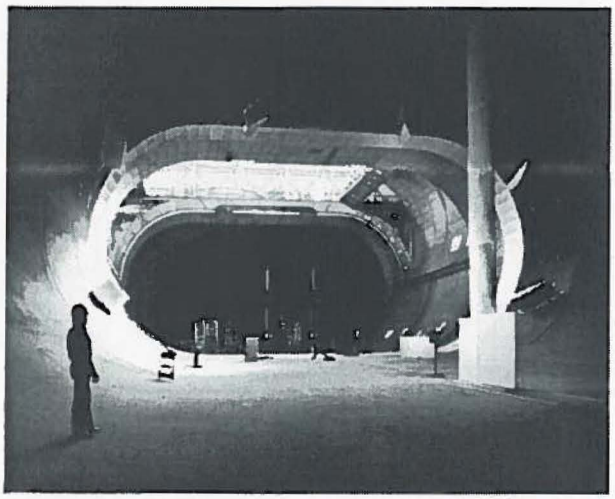

Figure 5. Vortex generators in 40x80 diffuser inlet; view looking upstream.

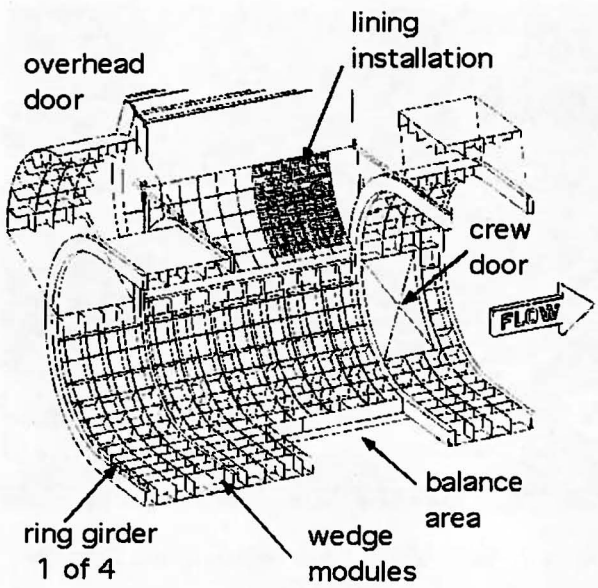

(a) Far view.

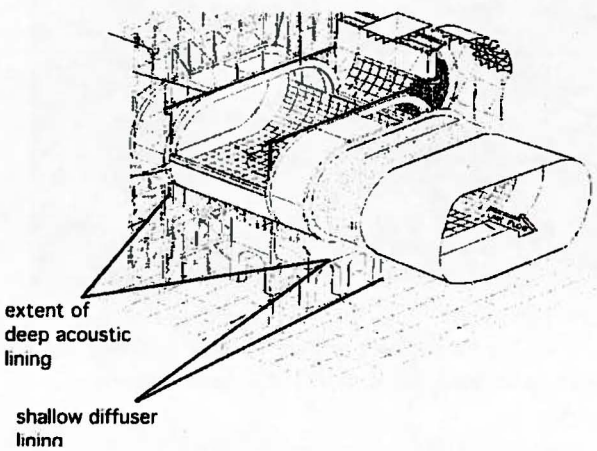

Figure 6. Lining location in wind tunnel.

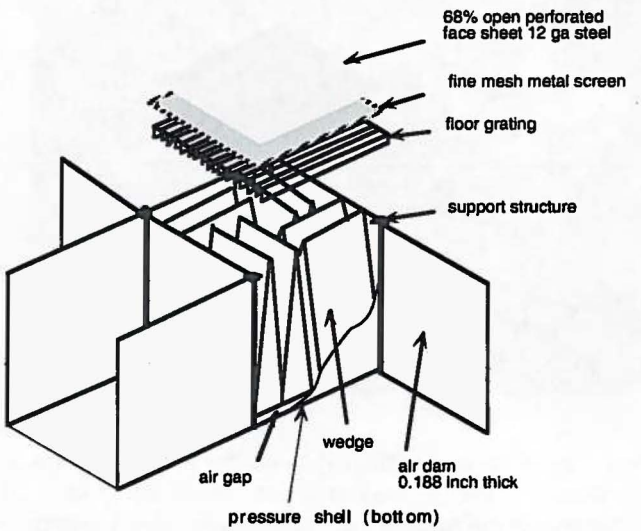

(b) Floor compartment detail.

Figure 7. Four-foot-square modular compartments that contain wedges and flow/lining interface.

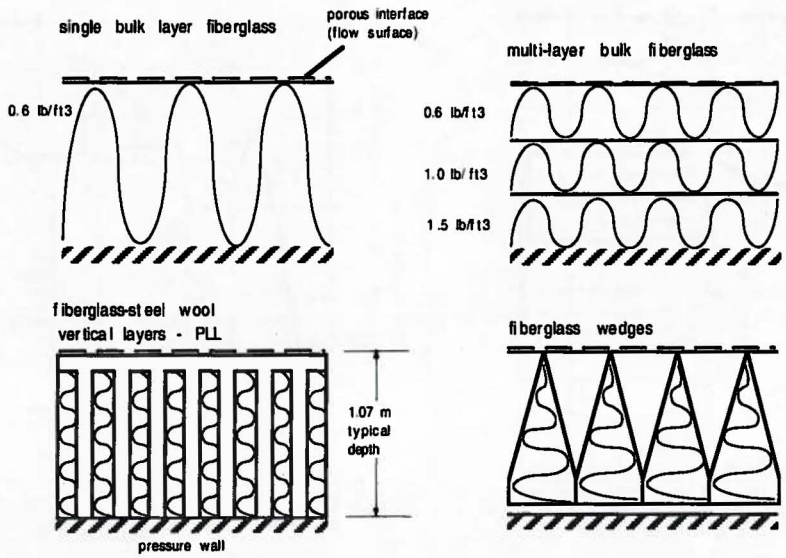

Figure 8. Four conceptual designs considered for the 40x80 lining

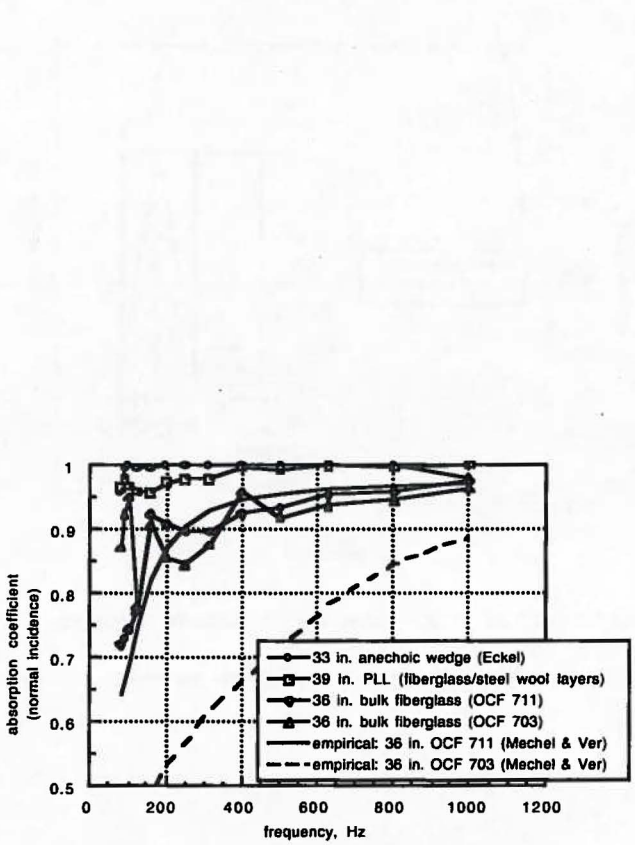

(a) Absorption coefficients

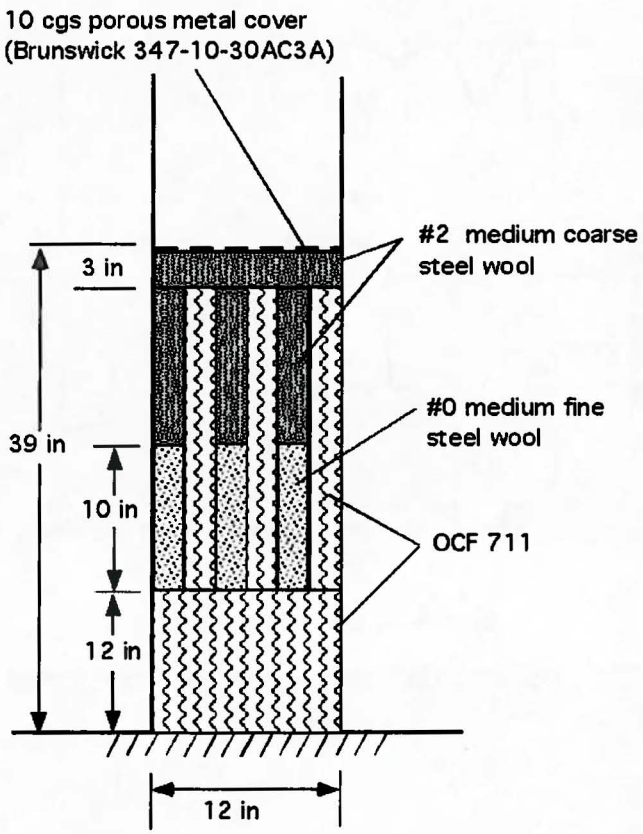

(b) Perpendicularly layered lining (PLL).

Figure 9. Performance of four candidate uncovered linings as measured in a 12-in.-square impedance tube (ref. 8). The fiberglass wedge composition was not determined. The bulk fiberglass was installed in 2-in. layers stacked parallel to the tube. A typical PLL geometry is shown in figure 9(b).

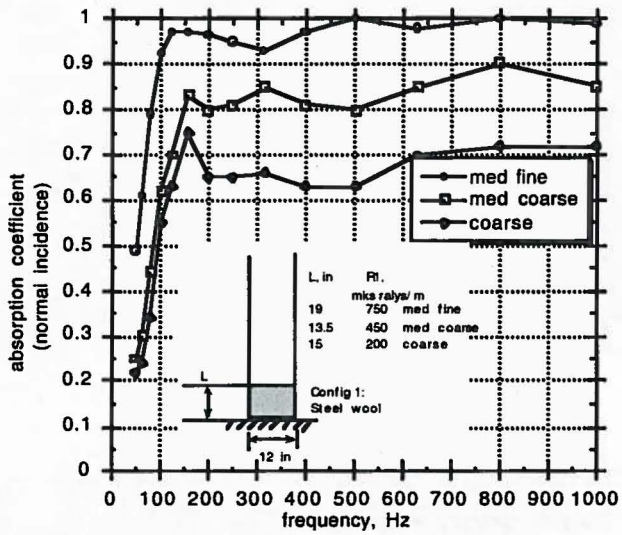

(a) Steel wool of various coarseness.

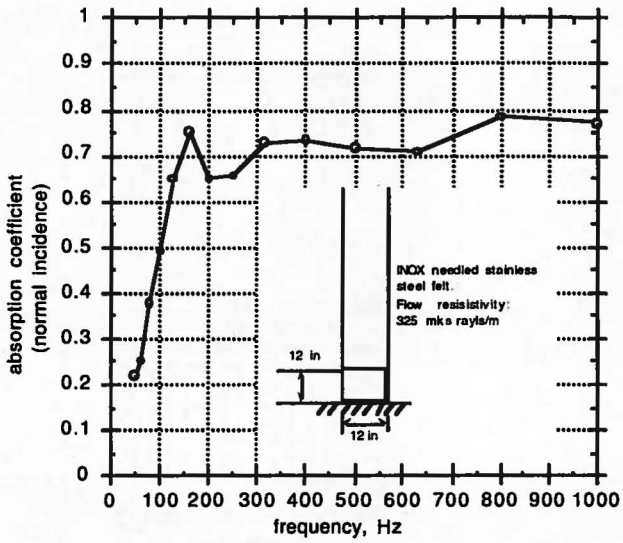

(c) Needled stainless steel felt.

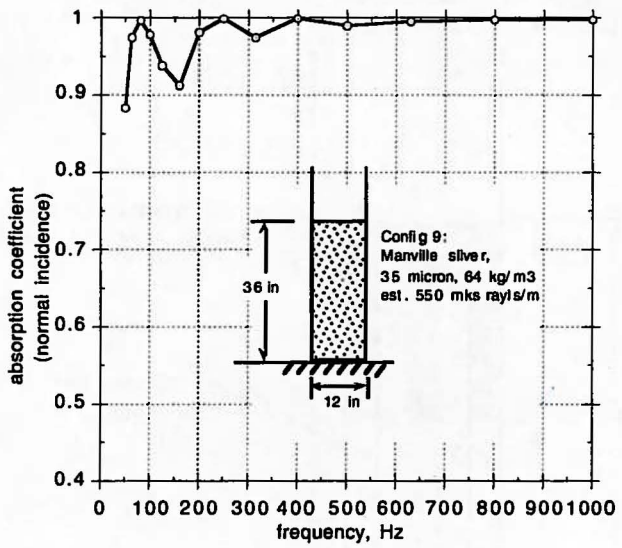

(b) Manville sliver fiberglass.

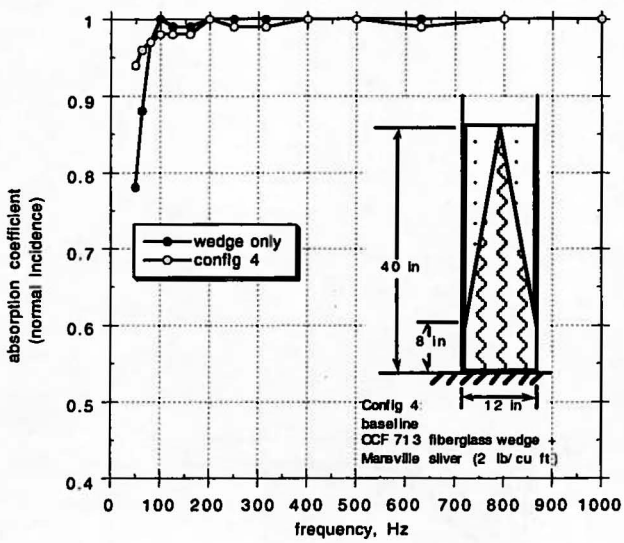

(d) Manville sliver fiberglass packed around a wedge.

Figure 10. Low-frequency absorption of single-layer bulk material. (Note variation in material depth.)

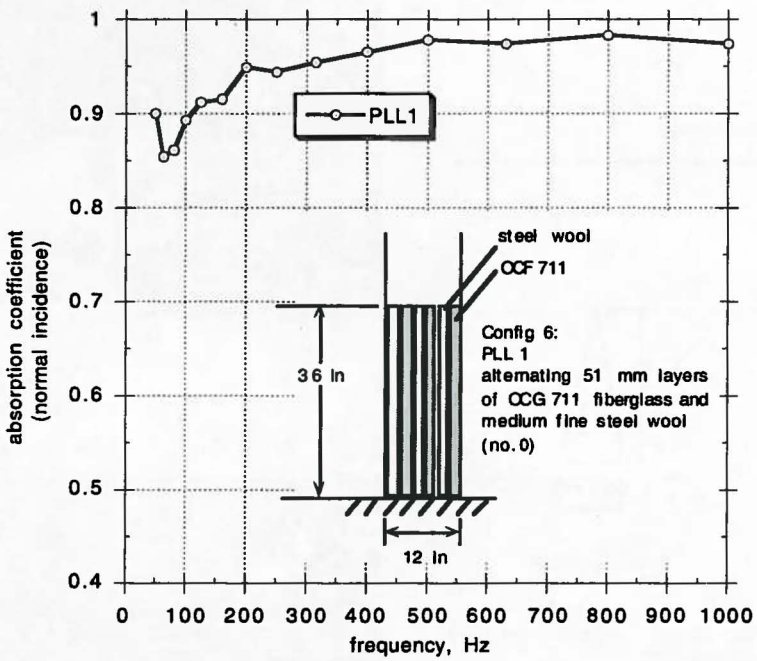

(a) Layers of fiberglass and steel wool.

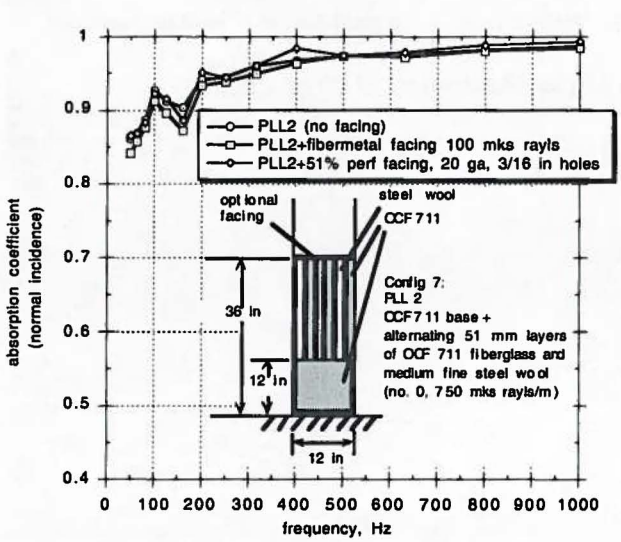

(b) Single layer base and facings incorporated.

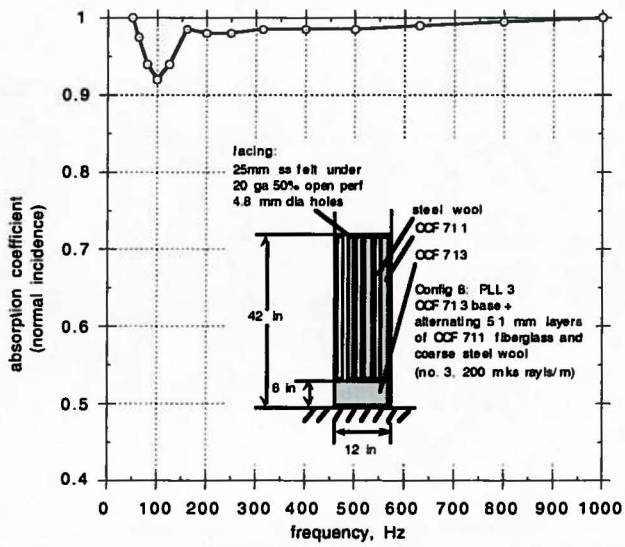

(c) Coarse steel wool in PLL.

Figure 11. Performance of perpendicular layer lining.

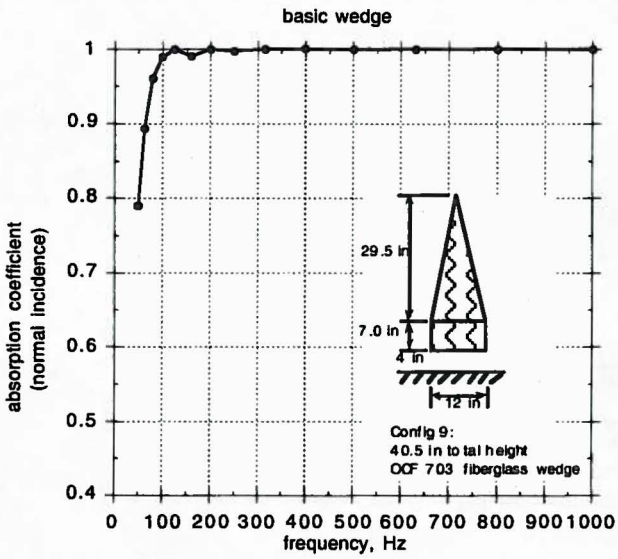

(a) Acoustic performance in impedance tube.

(b) Wedges used in coupon test in 40x80 test section.

Figure 12. Baseline OCF 703 fiberglass wedge with air gap. Resistivity: 27,000 mks rayls/m.

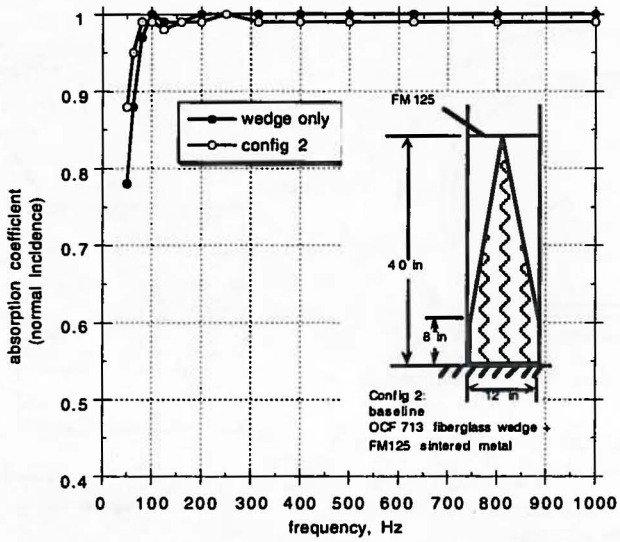

(a) Technetics FM125 sintered-metal interface.

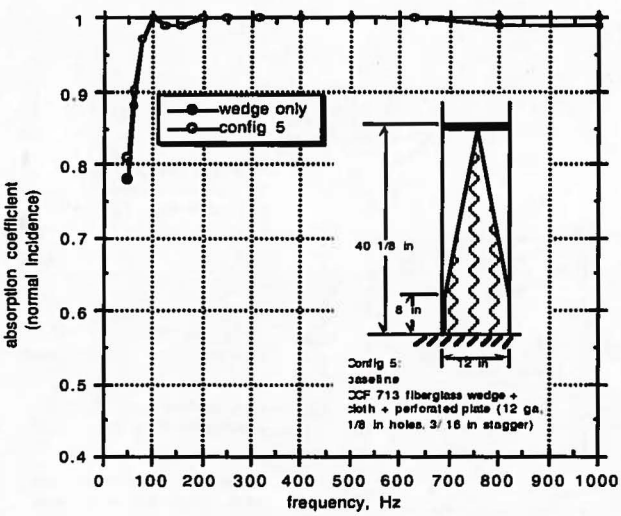

(b) Perforated 12 gauge plate (40%-open area) with cloth below plate.

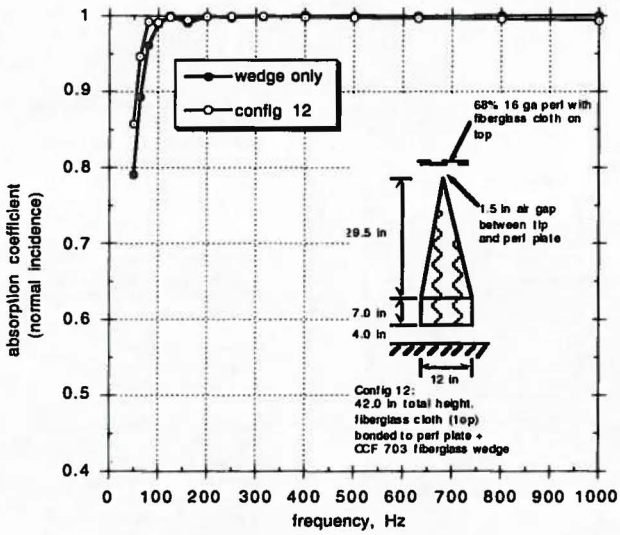

(c) 68%-open perforated 16 gauge plate with fiberglass cloth on top.

Figure 13. Low-frequency sound absorption of OCF 713 fiberglass baseline wedge with various simulated lining/flow interfaces without grating.

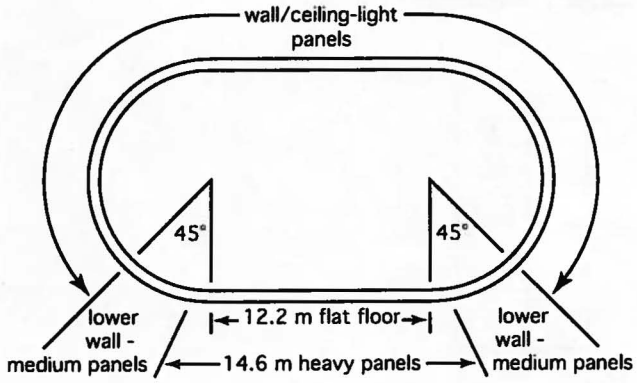

Figure 14. Location of floor, wall, and ceiling flow/interface panels. The floor panels are designed to support personnel and equipment. The lower wall panels are to support personnel only.

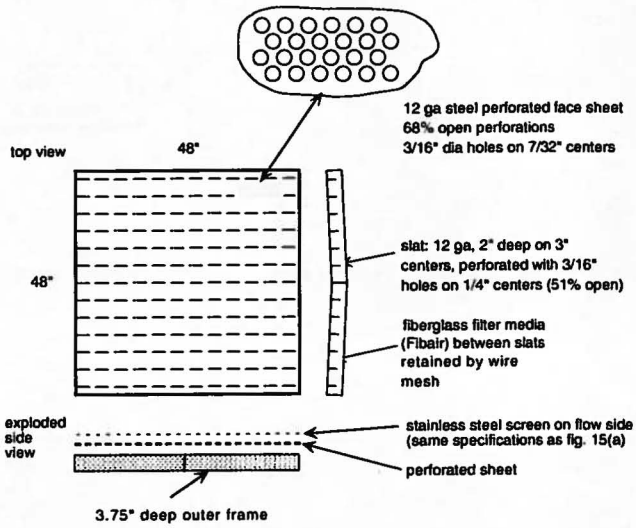

(b) Lower wall panel; two flat sections are used to approximate the local wall curvature.

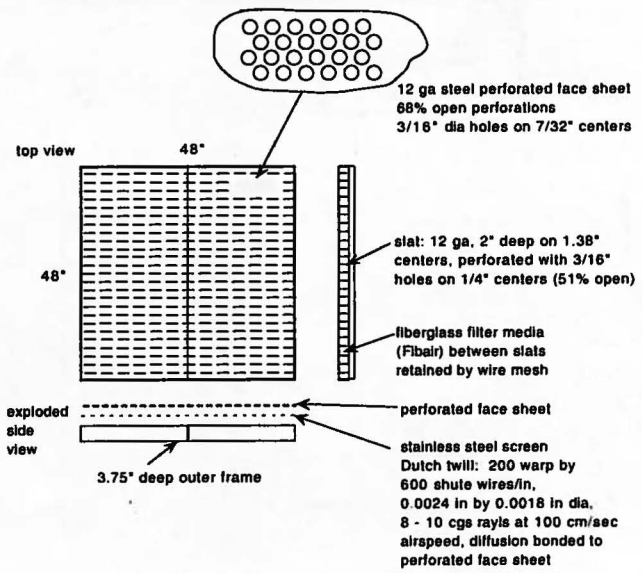

(a) Floor panel.

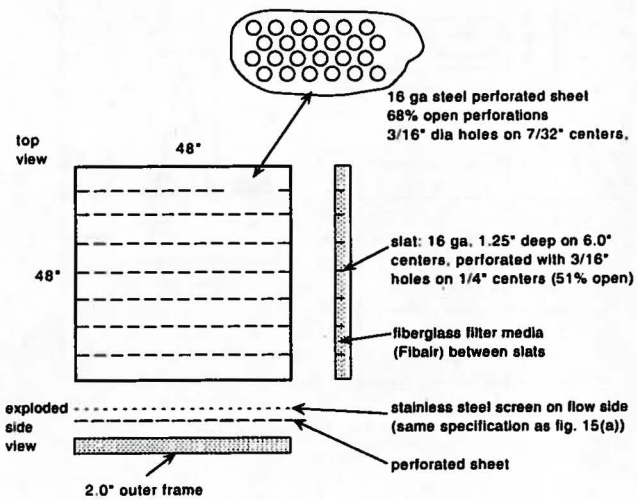

(c) Ceiling panel; upper wall panel is similar with kink in outer frame as shown in figure 15(b)

Figure 15. Typical grating panel and porous face sheet.

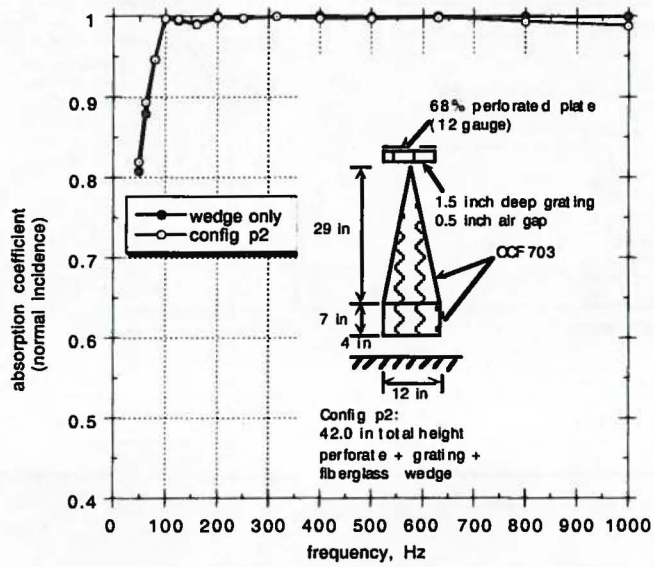

(a) Floor grating with perforated sheet above.

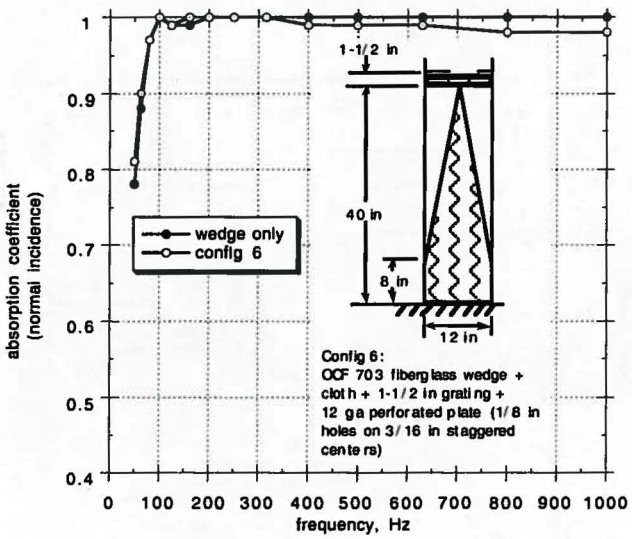

(b) Floor grating with cloth under grating.

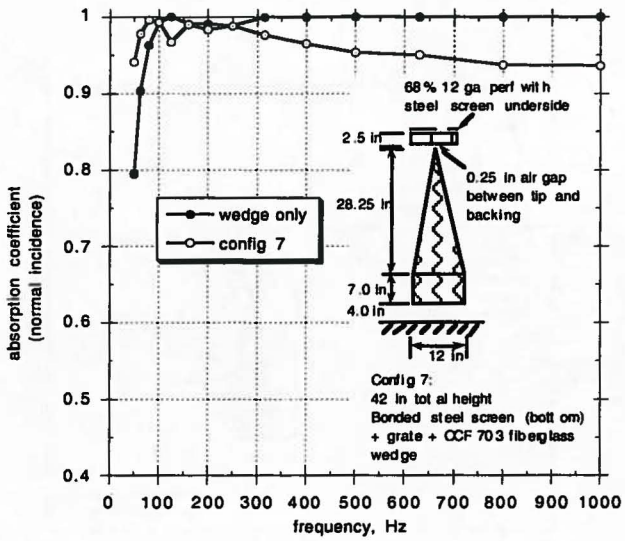

(c) Floor grating with stainless-steel screen below perforated sheet (Rf = 25 cgs rayls for performance plus screen).

Figure 16. Effect of floor flow/lining interface on low-frequency sound absorption. Wedge-only configuration is with or without 4-in. air gap under base as illustrated.

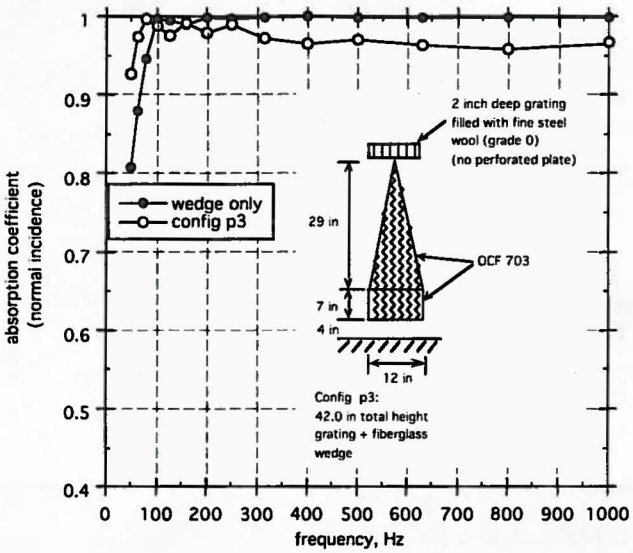

(a) Floor grating with fine steel wool between the slats.

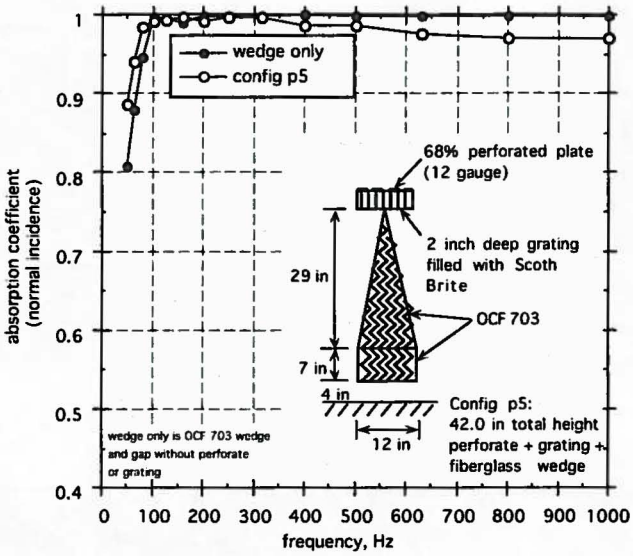

(c) Floor grating with Scotch Brite between slats, perforated sheet above. Scotch Brite is a highly porous stiff nylon mat coated with abresive resin used as a scrub (no screen).

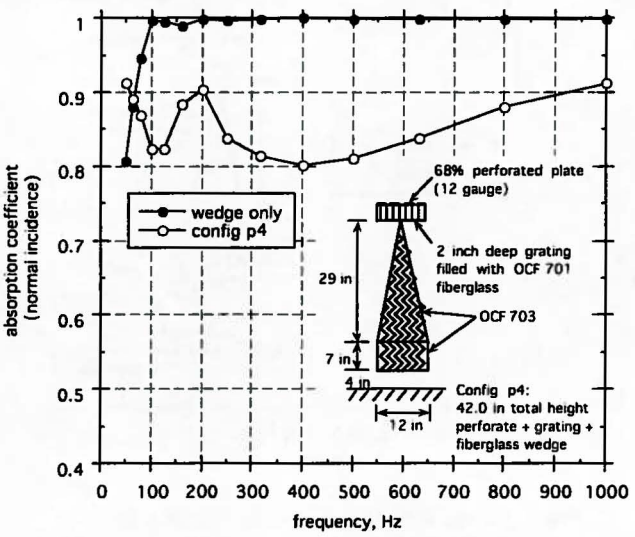

(b) Floor grating with OCF 701 fiberglass between slats, perforated sheet above.

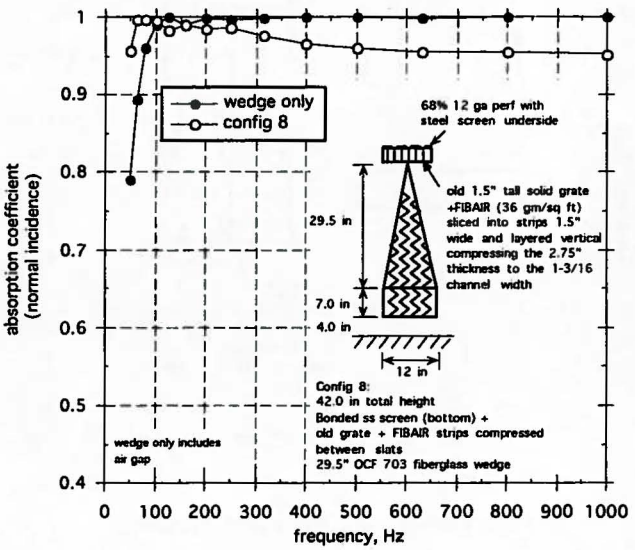

(d) Floor grating with Fibair between slats, perforated sheet with screen below (Rf = 25 cgs rayls for perforation plus screen).

Figure 17. Effect of filler material between grates.

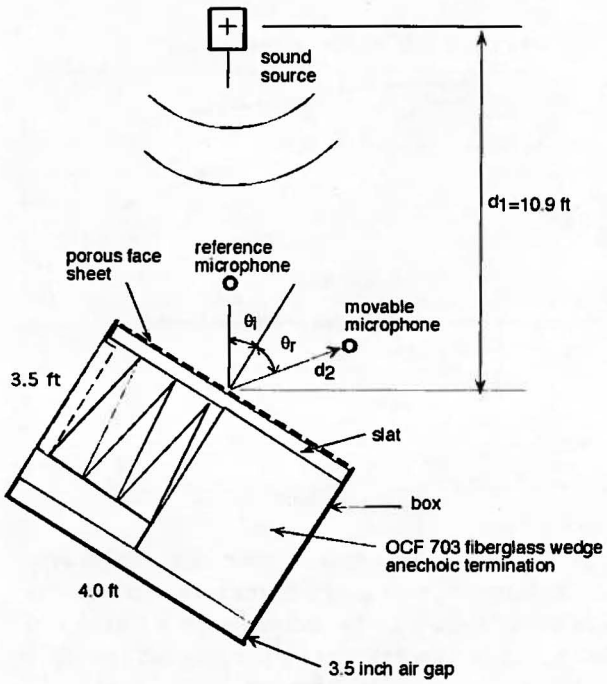

Figure 18. Wilby (ref. 15) test setup for two- microphone measurement of high-frequency reflections from test samples. Specimen box and reference microphone are 48 in. into page, movable microphone is 24 in. into page.

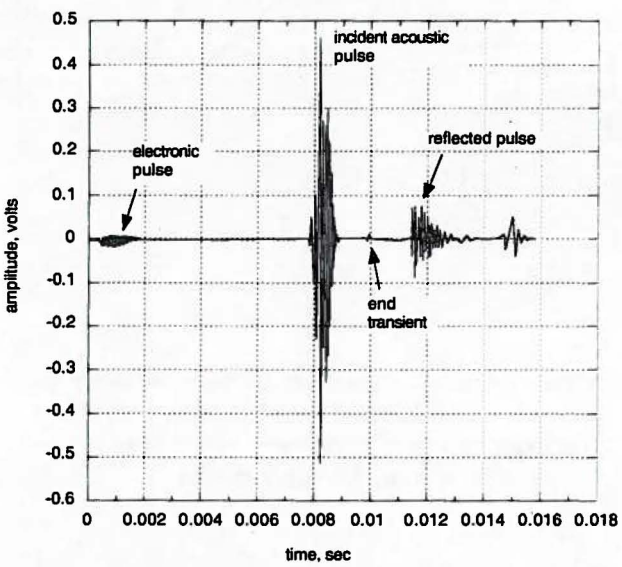

Figure 19. Typical chirp pulse and reflections. Time windows are applied to isolate the incident and reflected pulses.

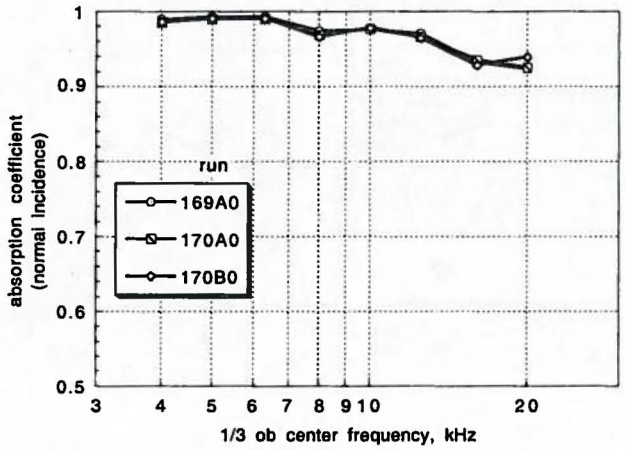

(a) Panel and test rig not moved between runs.

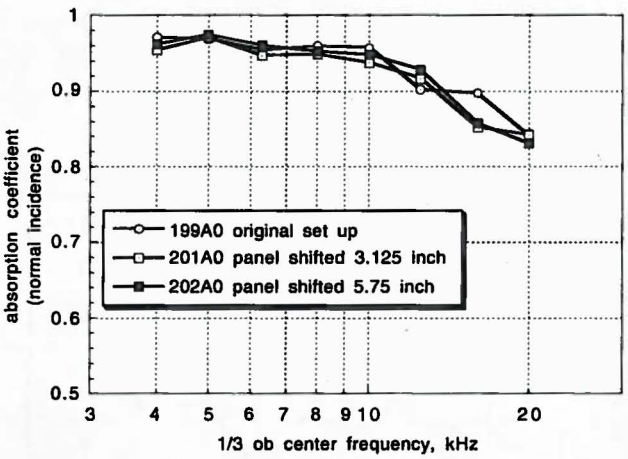

(b) Effect of shifting panel in test rig (production panel with screen).

Figure 20. Data repeatability from three runs. Ceiling configuration: 16-ga, 68%-open perforated plate without screen, 2-in. slats with Fibair between slats. (Note: figs. a and b are different panels.)

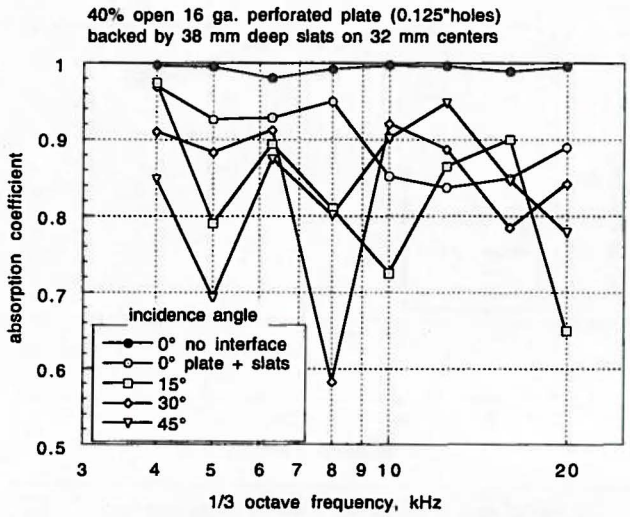

Figure 21. Sound absorption of Wilby (ref. 18) pulse-reflection test device with and without a 40%-open perforated plate over grating; acoustic incidence angles from 0° to 45° in a plane perpendicular to the grating slats.

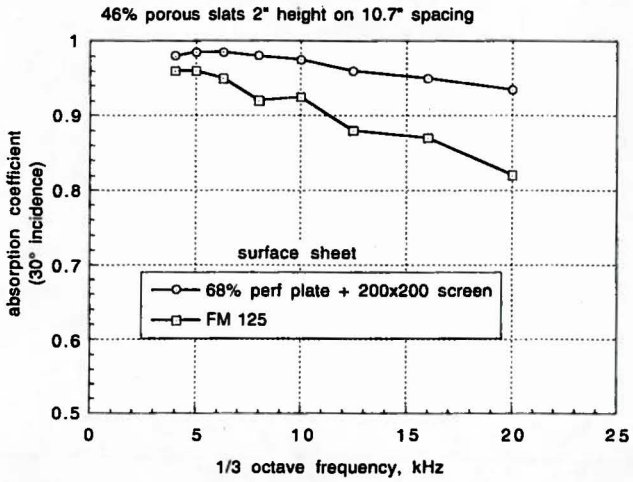

Figure 23. Comparison of perforated plate/screen and FM 125 feltmetal, both over a porous wall grating. The 16-gauge 68%-open perforated plate had a 200 by 200 wires/inch screen on top. The FM125 was laid directly on the wall grating.

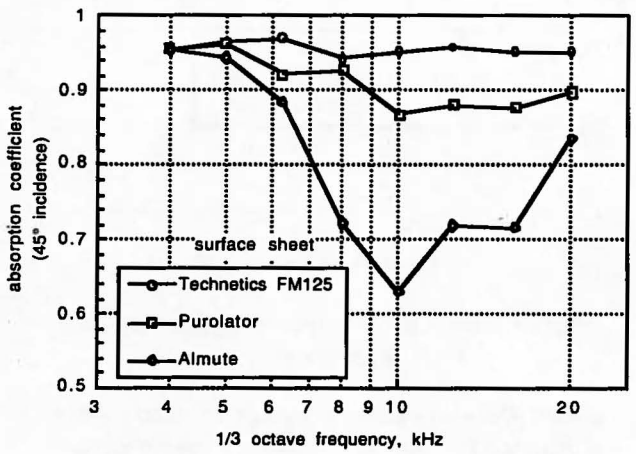

Figure 22. Sound absorption of Wilby (ref. 18) test lining (45°) with different porous metal surface coverings: Technetics FM125 feltmetal (10 cgs rayls); Purolator Poroplate, (10 cgs rayls); Almute (30 cgs rayls).

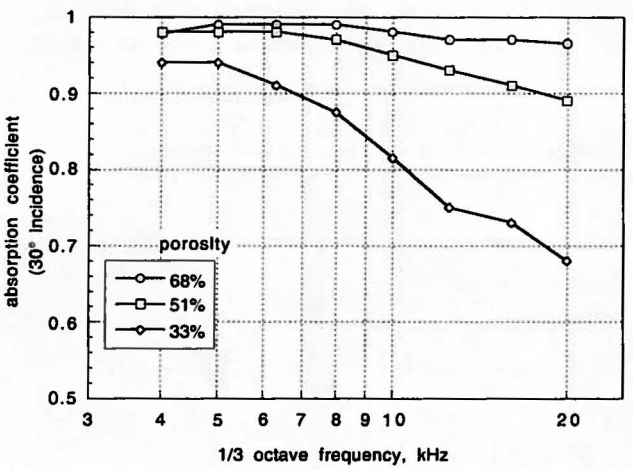

Figure 24. Effect of porosity on high-frequency absorption of a 0.0625-in.-thick (1.59 mm, 16 ga) perforated plate; hole diameter was 0.1875-in. (4.76 mm). No support slats.

Figure 25. Photo of 68%-open perforated plate with 0.1875-in. (4.76 mm) diameter holes on 0.217 inch (5.51 mm) staggered centers; A36 steel sheet.

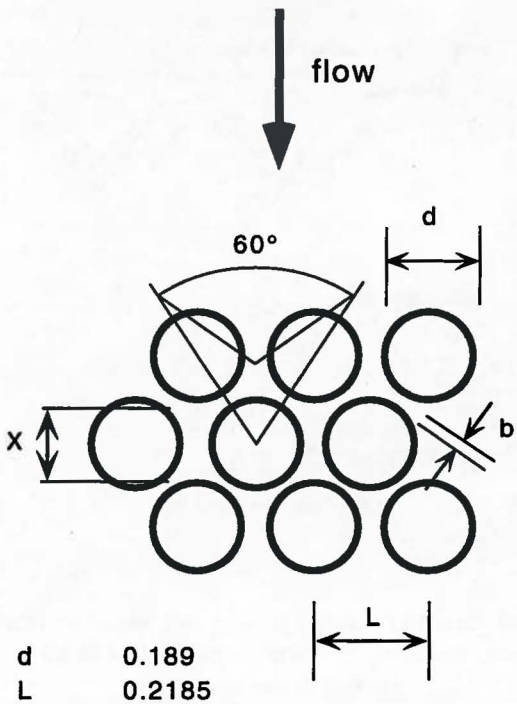

d	0.189
L	0.2185
b	0.0295
X	0.187
P	67.9%

dimensions in inches
d and L are specified, b, X and P result
P = porosity

Figure 26. Lining-surface hole geometry for wall and ceiling perforated plate (12 and 16 gauge). (Nominal dimensions: geometry is distorted by punching process so that porosity can range from 65% to 68%.)

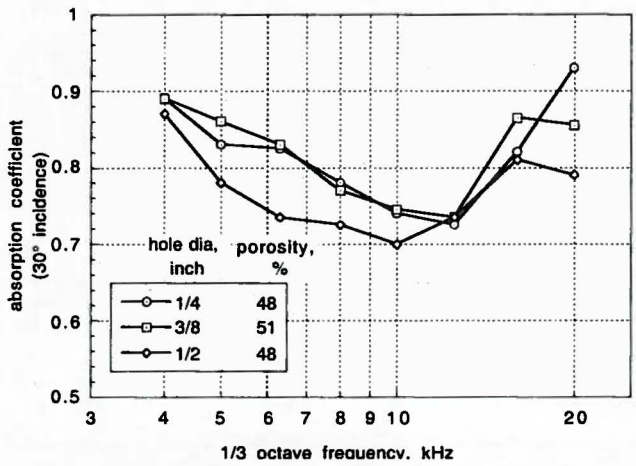

(a) 0.25-in.-thick plate.

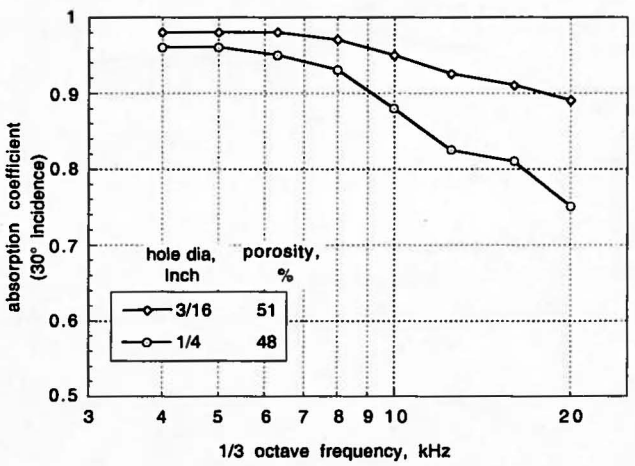

(b) 0.0625-in.-thick plate.

Figure 27. Effect of hole diameter on sound absorption of porous plate; porosity held to 48% - 51%, holes on staggered centers. No support slats.

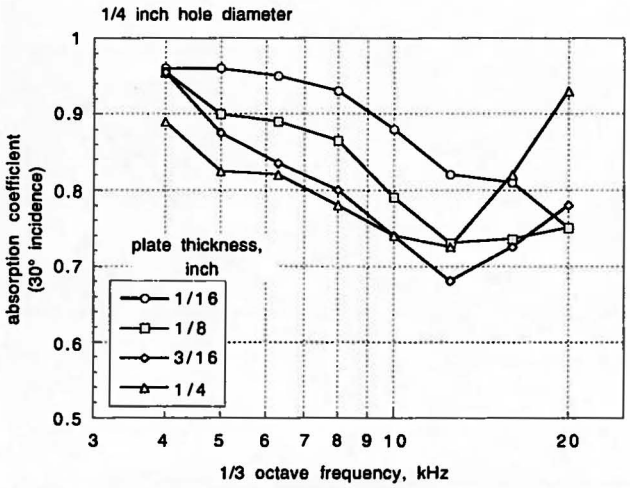

(a) 48% porous sheet.

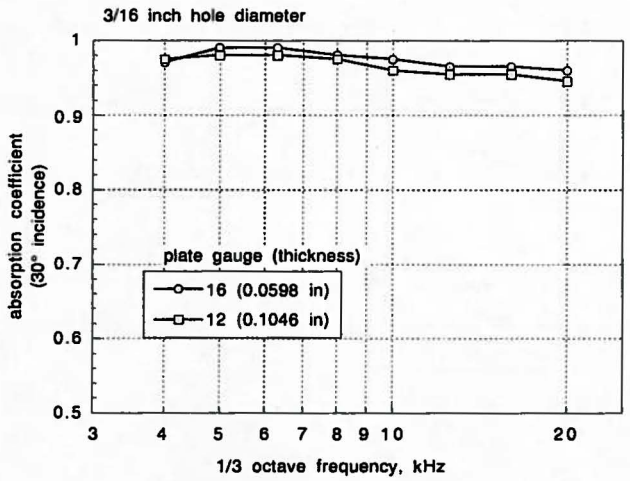

(b) 68% porous sheet.

Figure 28. Comparison of sound absorption coefficients for porous plates of different thicknesses; no support slats.

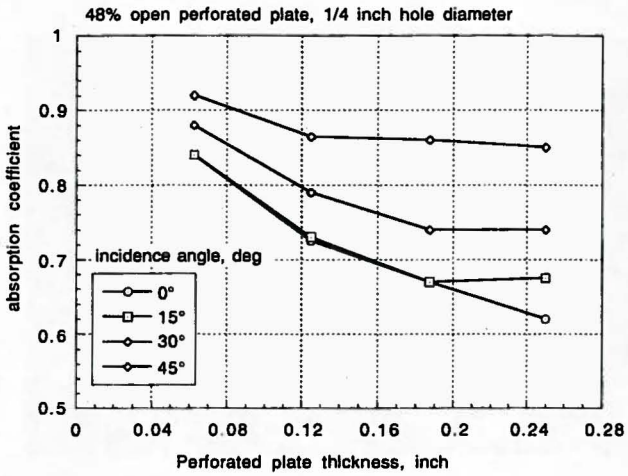

Figure 29. Effect of acoustic incidence angle and plate thickness on sound absorption at 10 kHz third octave band; no support slats.

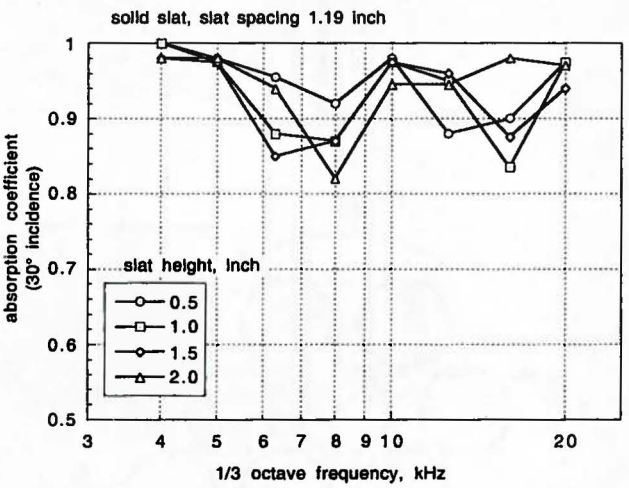

Figure 30. Effect of support grating slat height on sound absorption; sound ray in plane perpendicular to slats; no porous cover plate.

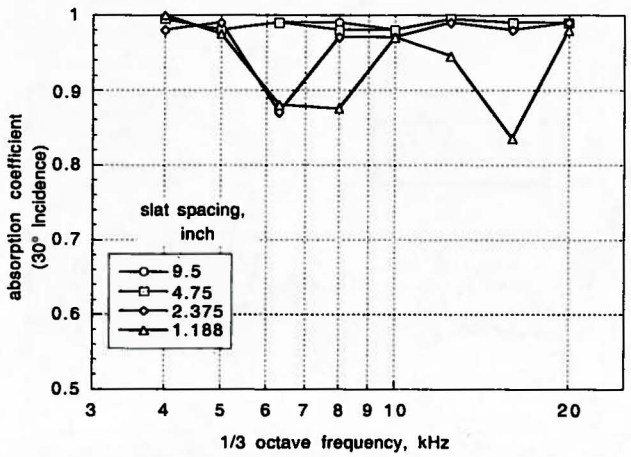

Figure 31. Effect of support grating slat spacing on sound absorption; no porous cover plate, solid slats 1 in. deep.

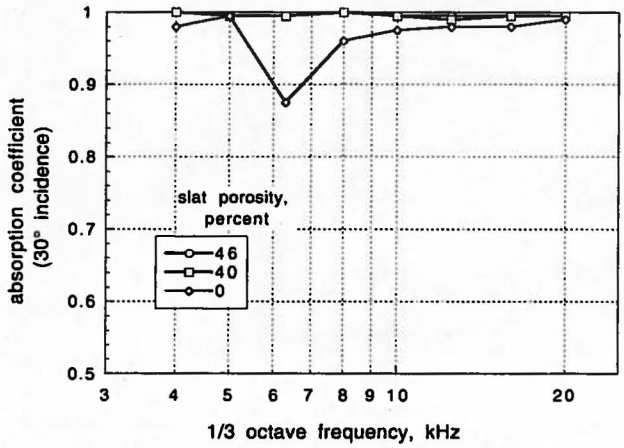

Figure 33. Effect of grating slat porosity on sound absorption; no porous cover, slats 1 in. deep on 2.375-in. spacing.

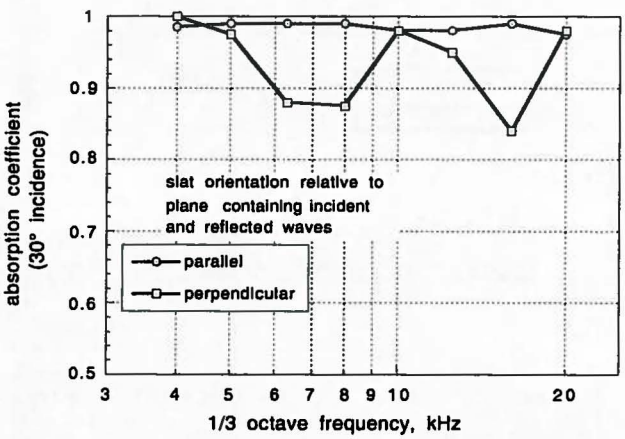

Figure 32. Effect of grating orientation relative to plane containing acoustic incidence and reflected rays; no porous cover plate, solid slats 1 in. deep on 1.19-in. centers.

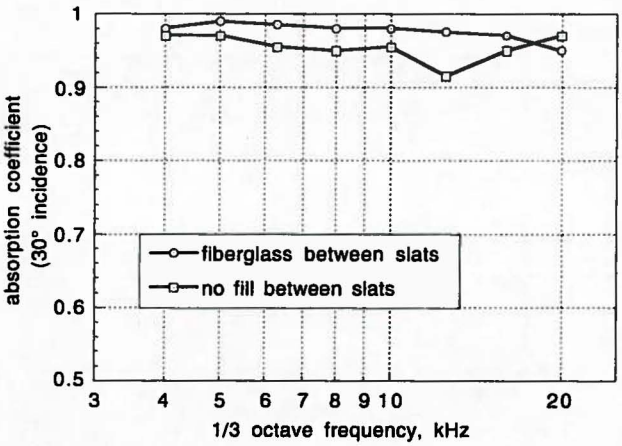

(a) OCF 701 fiberglass filler, 3-in. deep,12 gauge 68% porous performance plate, 63%-porous slats 3 in. height on 1.19 in. spacing

Figure 34. Effect of bulk material between grating slats on sound absorption; screen on top of perforated plate.

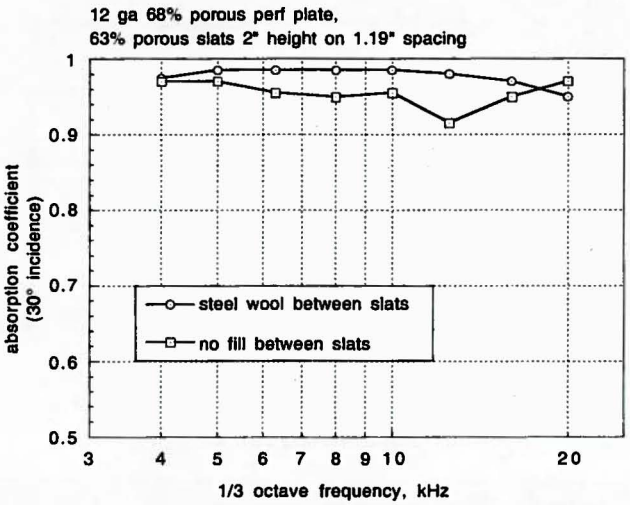

(b) Stainless steel wool filler (fine grade 0, 0.178 - 0.241 mm wire diameter).

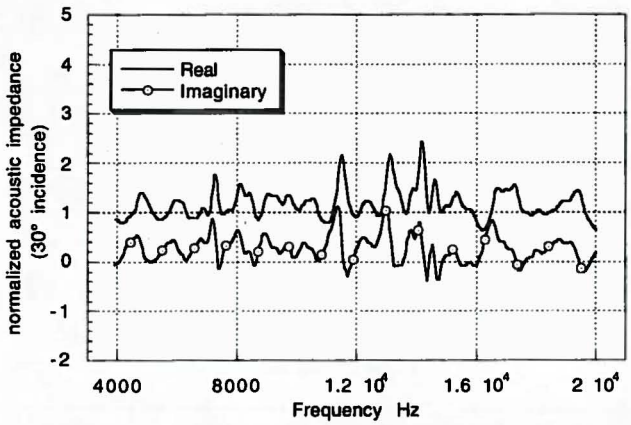

(d) Impedance normalized by ρc, no fill between grating slats.

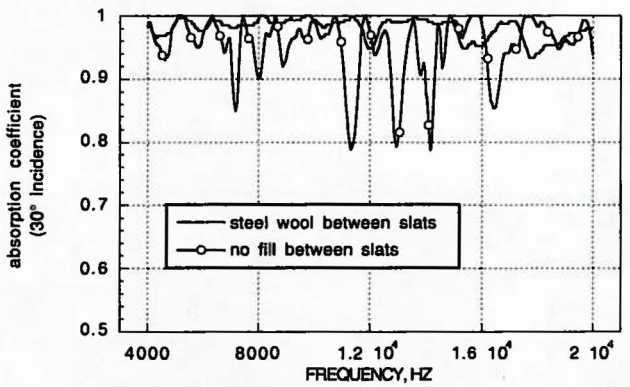

(c) Narrowband absorption coefficients.

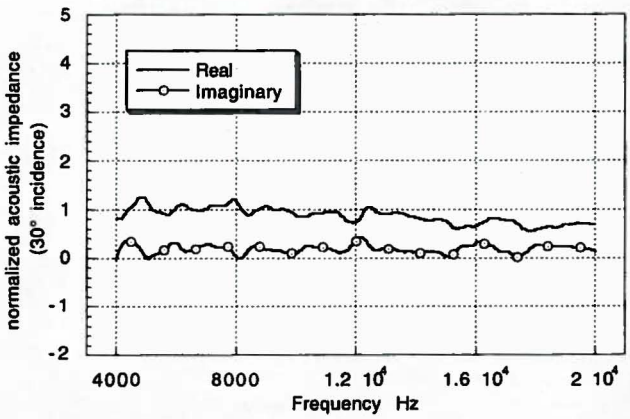

e) Impedance normalized by ρc, steel wool between slats.

Figure 34. Concluded.

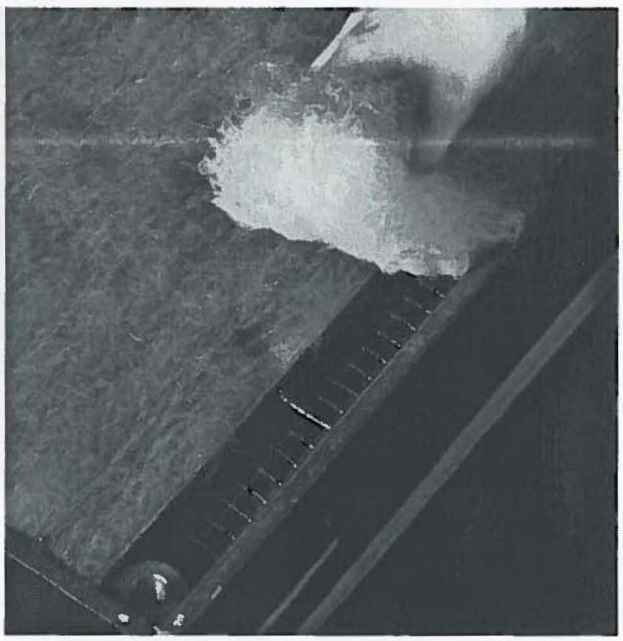

(a) Floor grating (AC94-0071-736).

(b) Wall grating (AC94-0071-734).

Figure 35. Fibair lightweight fiberglass filter material placed between grating slats.

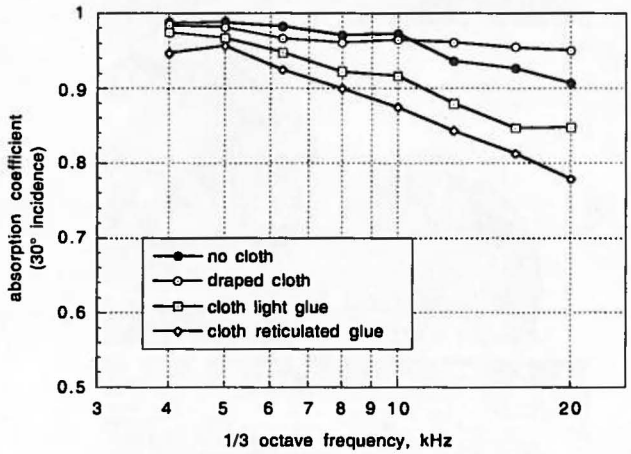

Figure 36. Deleterious effect of fiberglass cloth with adhesive below porous surface layer (12 gauge, 68%-open plate over 1-in. perforated slats at 9.5-in. spacing)

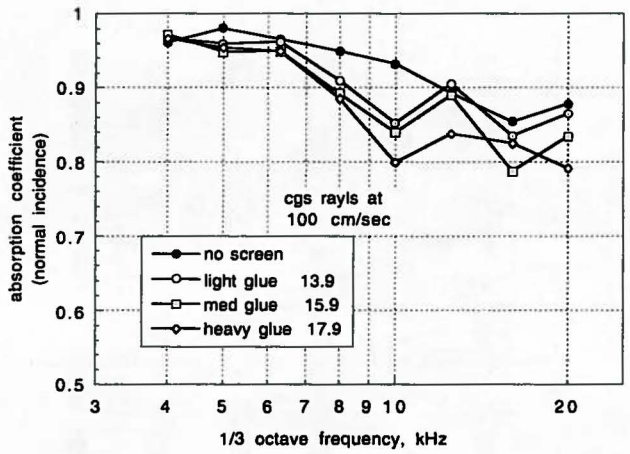

Figure 37. Effect of adhesive on sound absorption with 68%-open perforated plate and wire mesh screen glued to the wedge side of a 12-gauge plate. Screen 200x600 mesh, 0.061 mm and 0.046 mm dia warp and shute, twilled Dutch weave, 26 micron particle capture, 8-10 cgs rayls flow resistance.

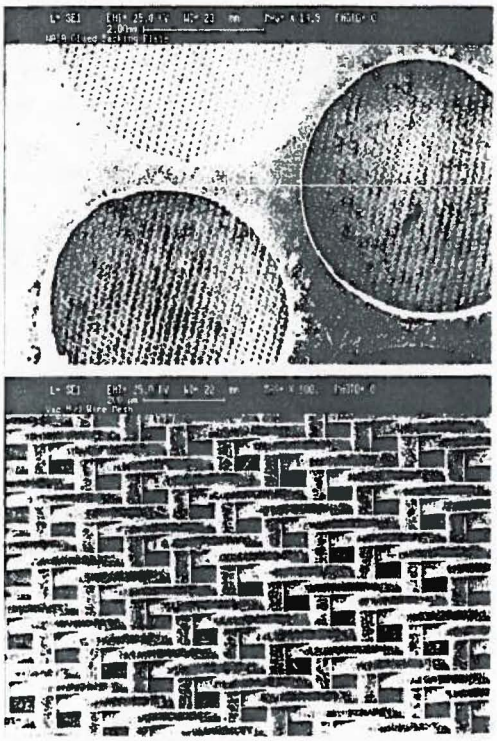

(a) Magnified view of screen bonded to perforated plate.

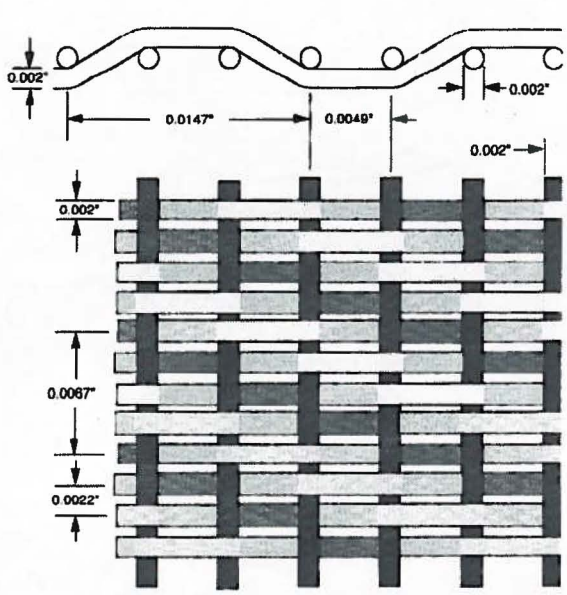

(b) Screen weave size.

Figure 38. Stainless-steel screen geometry.

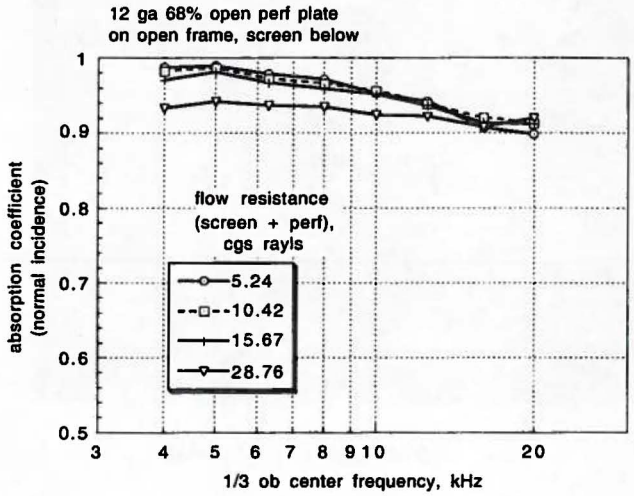

(a) 12-gauge 68%-perforated plate, screen below plate.

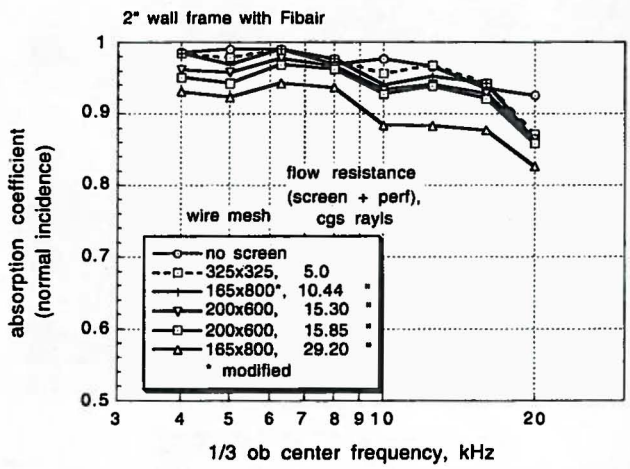

(b) 16-gauge 68%-perforated plate (screen above plate).

Figure 39. Sound absorption of diffusion bonded plate/ screen over lining with various values of flow resistance created by variations in screen mesh geometry.

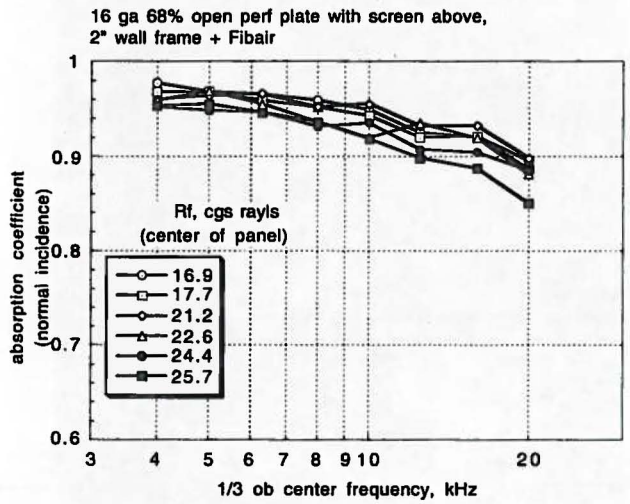

(a) a versus frequency.

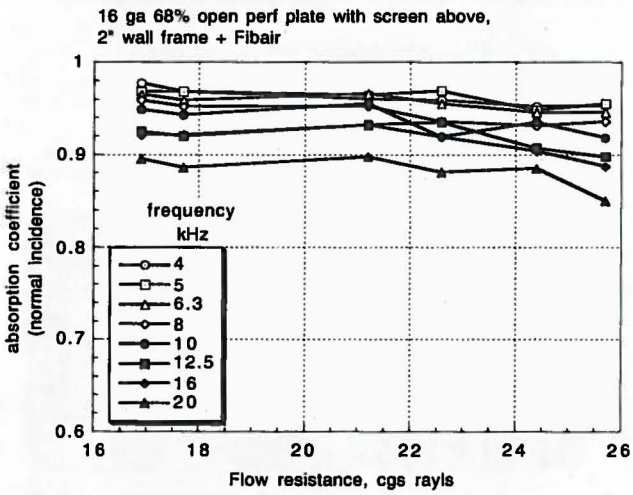

(b) a versus flow resistance (cross-plot of (a)).

Figure 40. Sound absorption of diffusion-bonded plate/screen over lining with various values of flow resistance. The screen mesh was common for all curves. Screen above perforated plate.

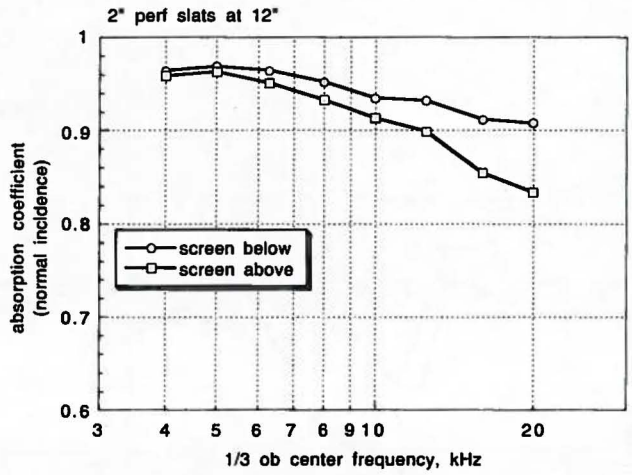

Figure 41. Effect of screen position on performance of 12-gauge floor panel, 68% open; 2 in. perforated slats, 12 in.-slat spacing, no Fibair, 18 cgs rayls.

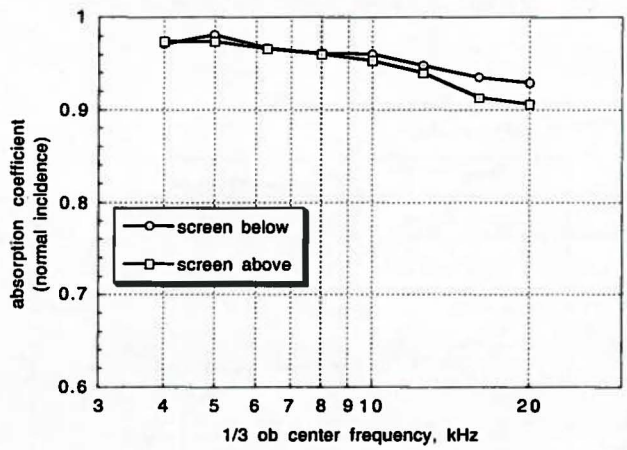

Figure 42. Effect of screen position on performance of 16-gauge 68%-open wall panel; 2-in. perforated slats, 12-in. slat spacing, no Fibair, 15.85 cgs rayls.

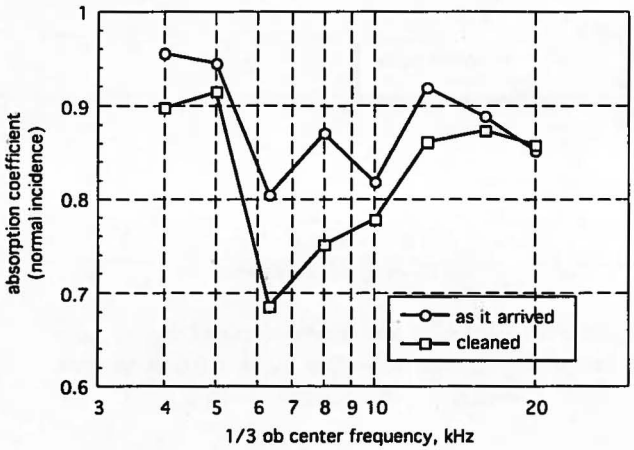

(a) Dirty production panel before and after cleaning.

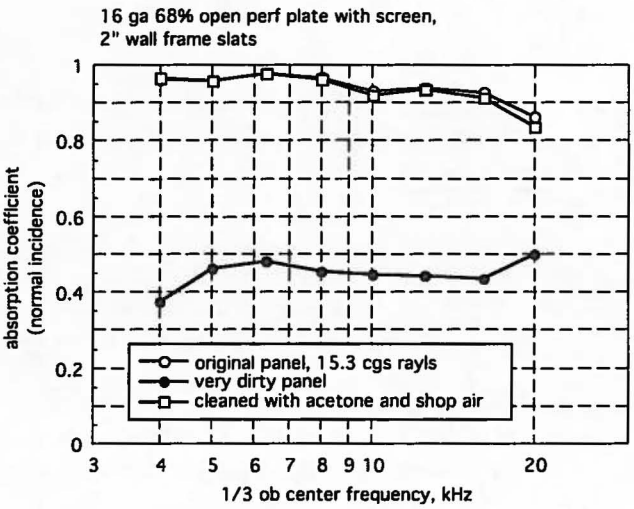

(b) Panel contaminated with jet fuel smoke and subsequently cleaned.

Figure 43. Effect on sound absorption of cleaning panels.

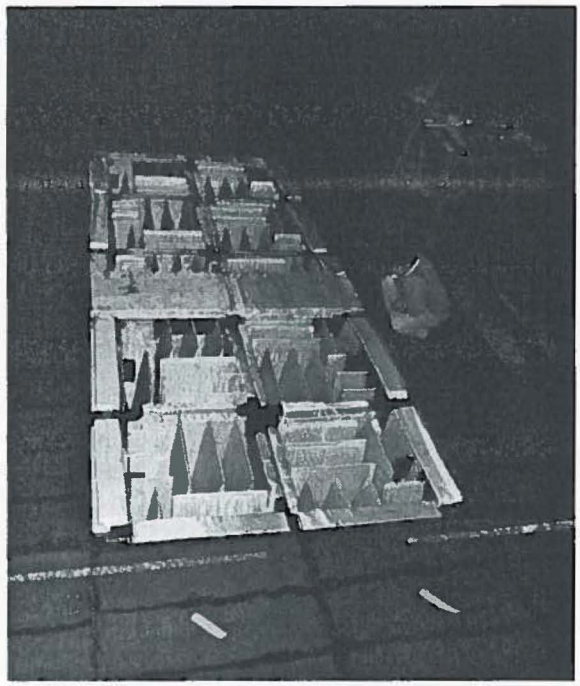

(a) Grating and porous cover removed.

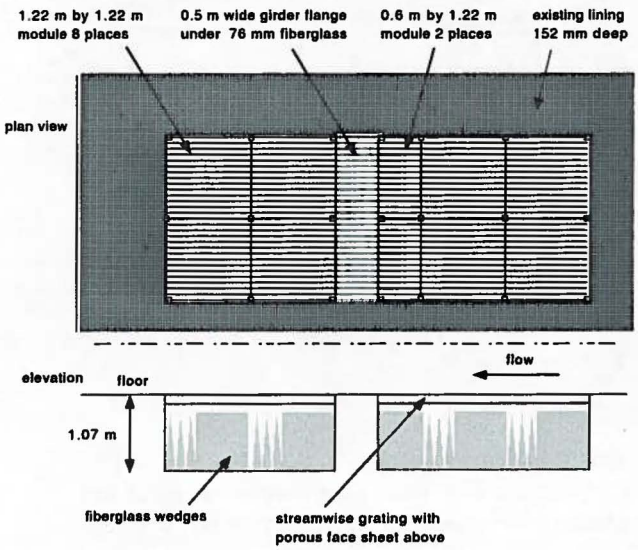

(b) Geometry.

Figure 44. Coupon modules mounted in 40x80 test section floor for aerodynamic and acoustic testing.

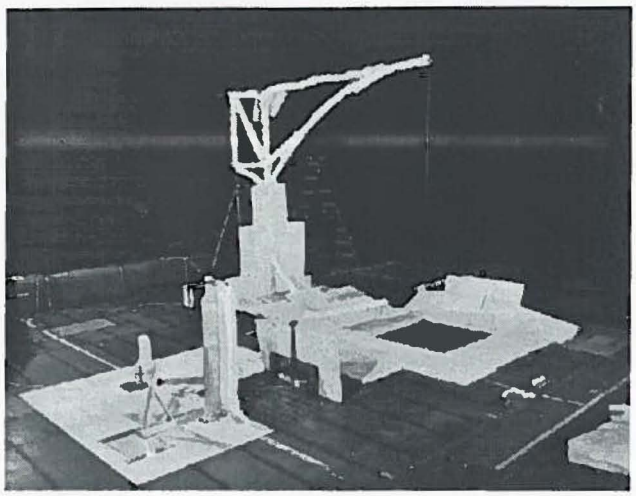

Figure 45. Coupon test rig setup for static sound absorption. Four loudspeakers are mounted on arc over test module. Fiberglass blanket was used to shield hard points outside test area.

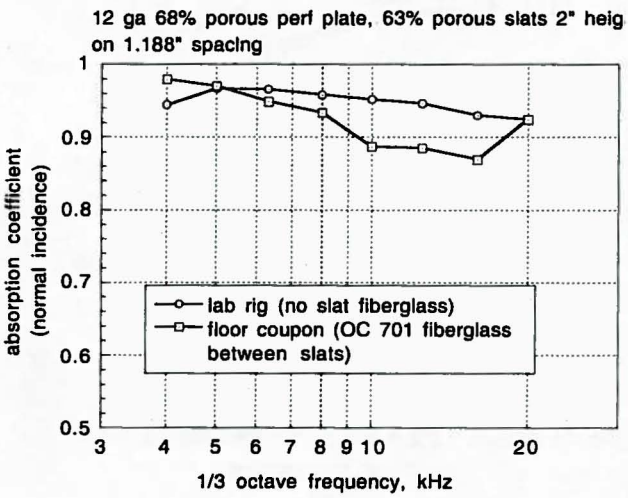

(a) Floor configuration (the lab rig sample had no fiberglass between the slats).

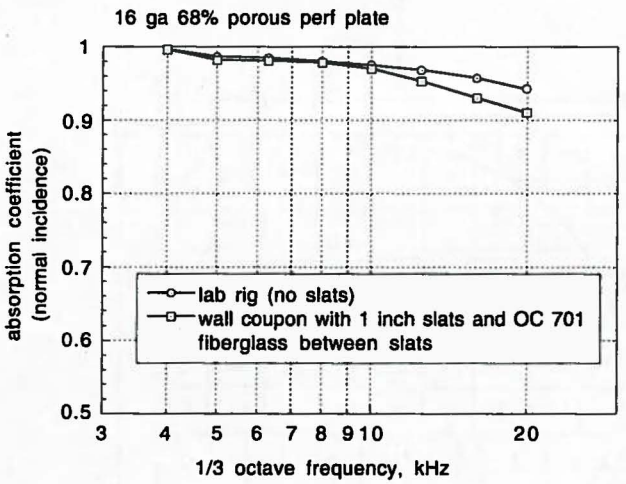

(b) Wall configuration (lab rig sample contained no slats).

Figure 46. A comparison of 40x80 coupon and laboratory test rig results. The OC 701 fiberglass between the slats was detrimental to sound absorption at high frequencies.

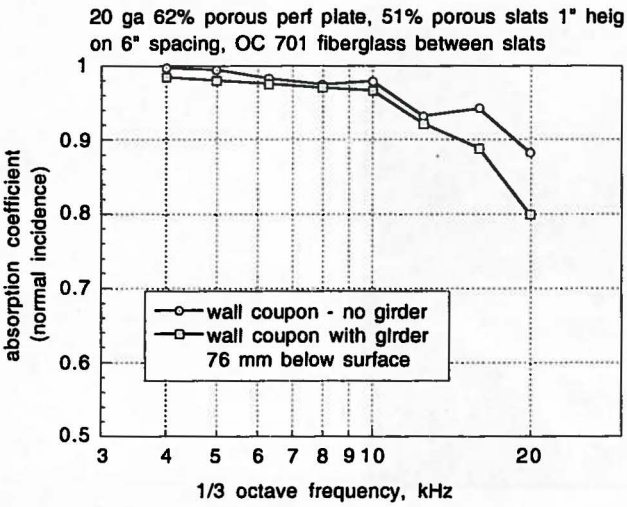

Figure 47. 40x80 wall coupon with and without a ring girder 6 in. (152 mm) below the flow surface. Ring girder was covered by OCF 701 fiberglass.

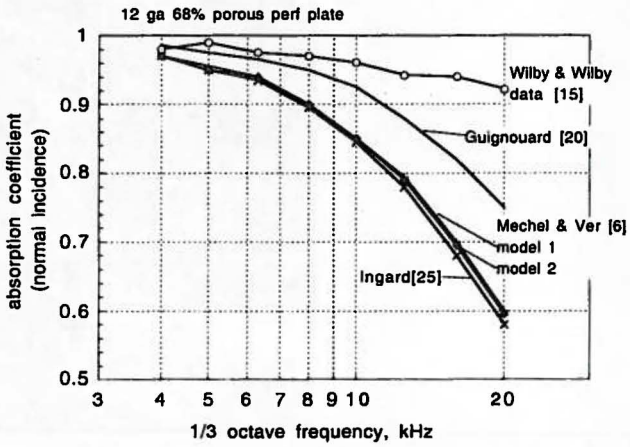

(a) 12 gauge, 68%-open perforated plate above an anechoic termination.

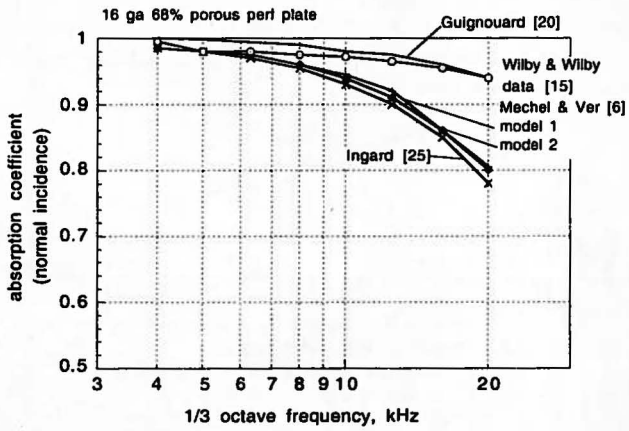

(b) 16 gauge, 68%-open perforated plate over an anechoic termination.

Figure 49. Comparison of predicted and measured high-frequency sound absorption. Four analytical models are plotted along with pulse-reflection data from Wilby and Wilby (ref. 18).

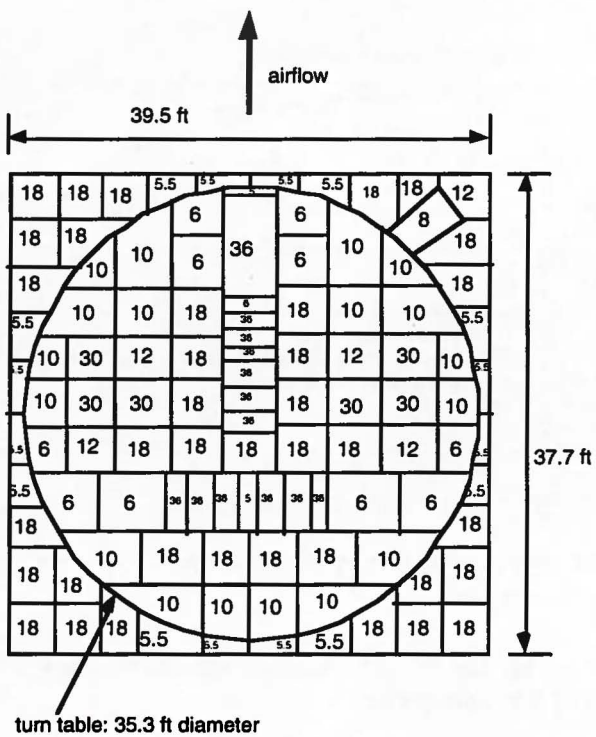

Figure 48. Plan of test section turntable showing depths (inches) of special lining modules in that area. Outside this area, the lining depth is generally 42 in.

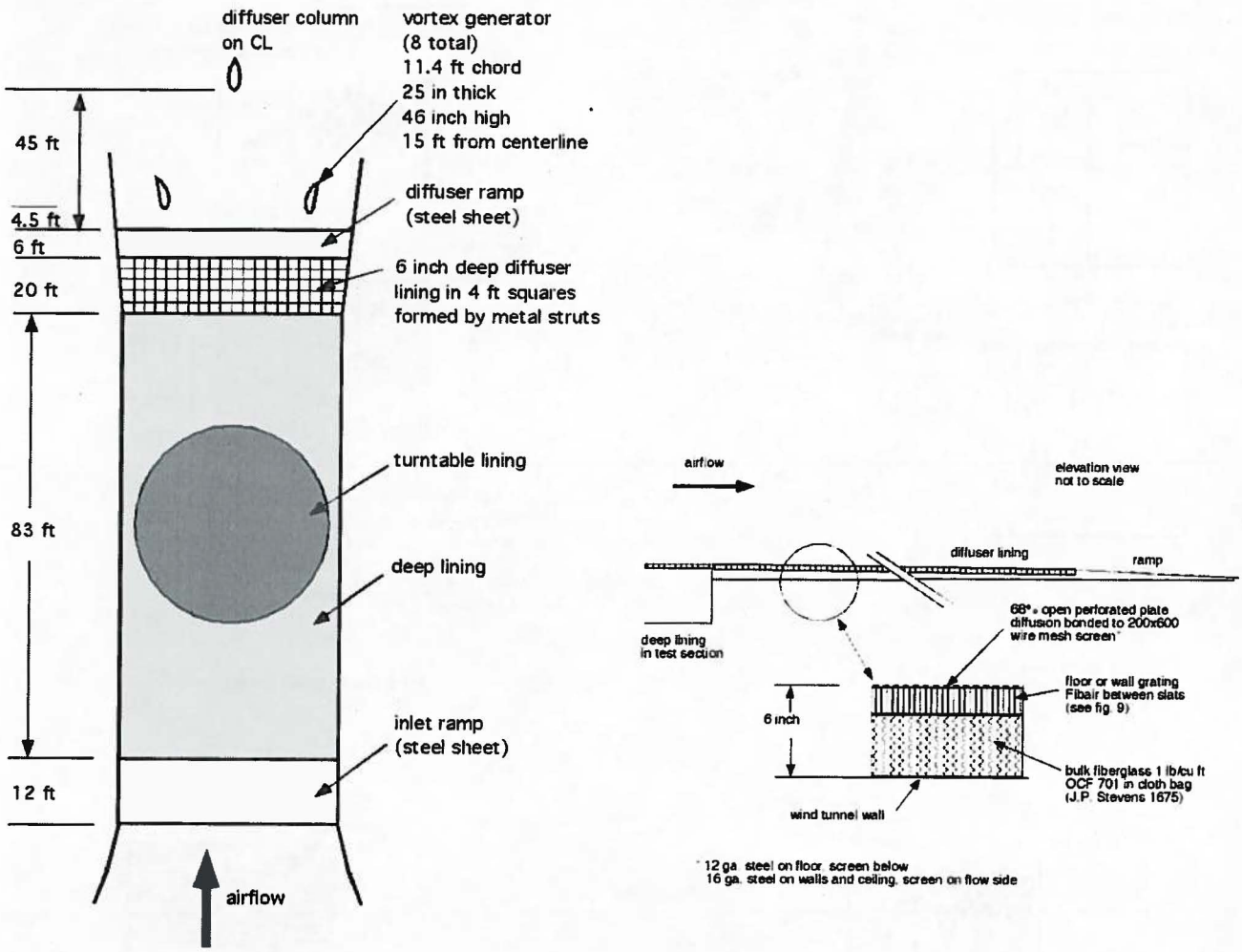

(a) Plan view of floor.

(b) Elevation.

Figure 50. The shallow lining in the diffuser inlet.

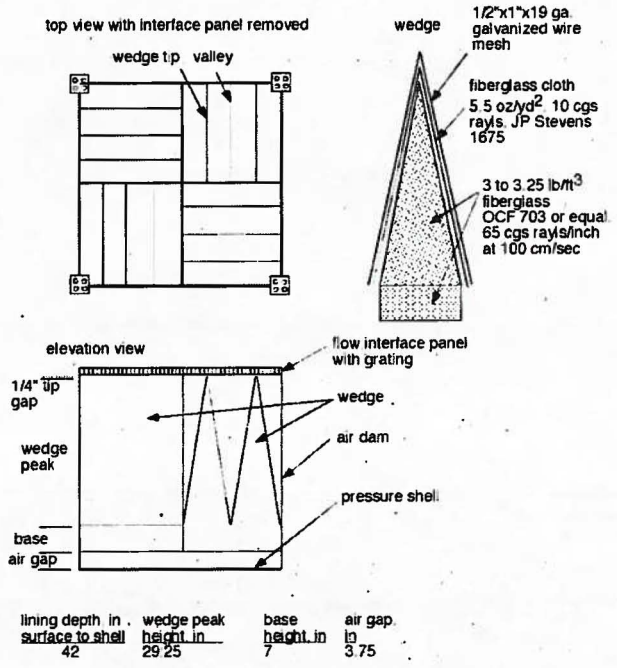

(a) Wedge detail.

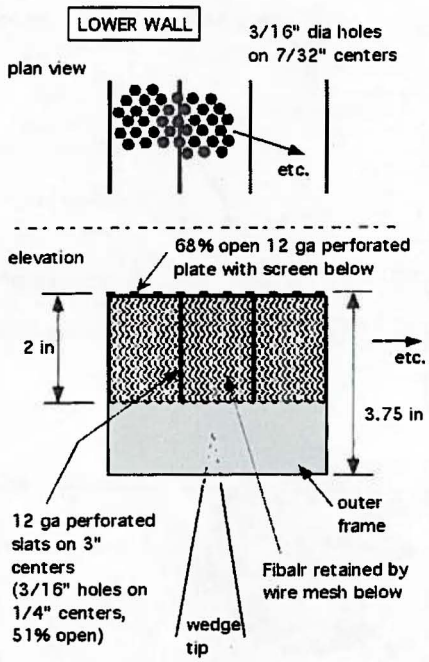

(c) Lower wall panel.

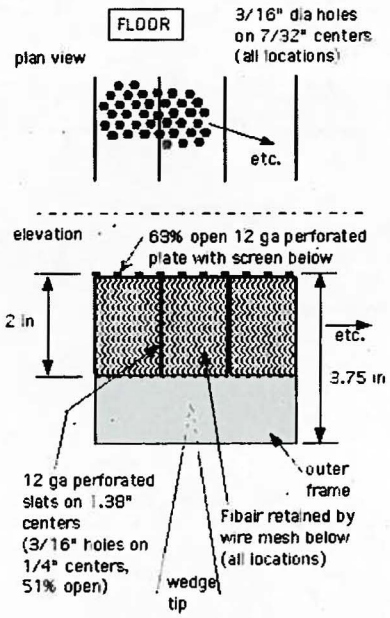

(b) Floor panel.

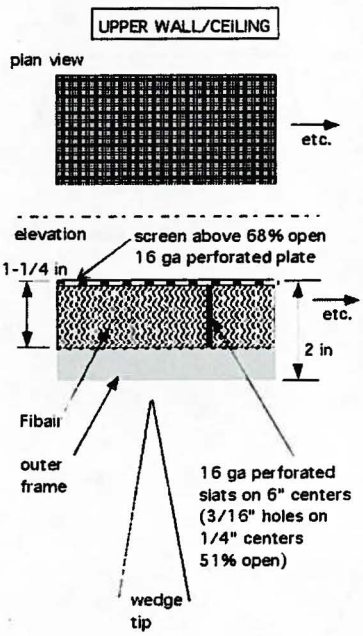

(d) Upper wall/ceiling panel.

Figure 51. Final design geometry and specifications.

REPORT DOCUMENTATION PAGE

Form Approved
OMB No. 0704-0188

1. AGENCY USE ONLY *(Leave blank)*	2. REPORT DATE	3. REPORT TYPE AND DATES COVERED
	November 2002	Technical Publication

4. TITLE AND SUBTITLE

Design and Development of a Deep Acoustic Lining for the 40- by 80-Foot Wind Tunnel Test Section

5. FUNDING NUMBERS

519-20-32

6. AUTHOR(S)

Paul T. Soderman, Fredric H. Schmitz,* Christopher S. Allen, Stephen M. Jaeger,** Joe N. Sacco, Marianne Mosher, and Julie A. Hayes†

7. PERFORMING ORGANIZATION NAME(S) AND ADDRESS(ES)

Ames Research Center, Moffett Field, CA 94035-1000; *University of Maryland, College Park, MD 20742; **AerospaceComputing, Inc., at Ames Research Center, Moffett Field, CA 94035-1000; and †Signalscape, Inc., Raleigh, NC 27606

8. PERFORMING ORGANIZATION REPORT NUMBER

A-0208163

9. SPONSORING/MONITORING AGENCY NAME(S) AND ADDRESS(ES)

National Aeronautics and Space Administration
Washington, DC 20546-0001

10. SPONSORING/MONITORING AGENCY REPORT NUMBER

NASA/TP—2002-211850

11. SUPPLEMENTARY NOTES

Point of Contact: Paul T. Soderman, Ames Research Center, MS 247-2, Moffett Field, CA 94035-1000
(650) 604-6675

12a. DISTRIBUTION/AVAILABILITY STATEMENT

Unclassified — Unlimited
Subject Category 09 Distribution: Standard
Availability: NASA CASI (301) 621-0390

12b. DISTRIBUTION CODE

13. ABSTRACT *(Maximum 200 words)*

The work described in this report has made effective use of design teams to build a state-of-the-art anechoic wind-tunnel facility. Many potential design solutions were evaluated using engineering analysis, and computational tools. Design alternatives were then evaluated using specially developed testing techniques. Large-scale coupon testing was then performed to develop confidence that the preferred design would meet the acoustic, aerodynamic, and structural objectives of the project. Finally, designs were frozen and the final product was installed in the wind tunnel.

The result of this technically ambitious project has been the creation of a unique acoustic wind tunnel. Its large test section (39 ft x 79 ft x 80 ft), potentially near-anechoic environment, and medium subsonic speed capability (M = 0.45) will support a full range of aeroacoustic testing—from rotorcraft and other vertical takeoff and landing aircraft to the takeoff/landing configurations of both subsonic and supersonic transports.

14. SUBJECT TERMS	15. NUMBER OF PAGES
Aeroacoustics, Wind tunnel acoustics, Duct lining	57
	16. PRICE CODE

17. SECURITY CLASSIFICATION OF REPORT	18. SECURITY CLASSIFICATION OF THIS PAGE	19. SECURITY CLASSIFICATION OF ABSTRACT	20. LIMITATION OF ABSTRACT
Unclassified	Unclassified	Unclassified	